

Mitogen-Activated Protein Kinase-Activated Protein Kinase 2 (MAPKAP-K2) as an Antiinflammatory Target: Discovery and in Vivo Activity of Selective Pyrazolo[1,5-*a*]pyrimidine Inhibitors Using a Focused Library and Structure-Based Optimization Approach[†]

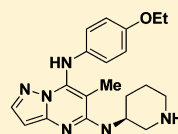
Tomomi Kosugi,[‡] Dale R. Mitchell,^{*,§} Aiko Fujino,[‡] Minoru Imai,[‡] Mika Kambe,[‡] Shinji Kobayashi,[‡] Hiroaki Makino,[‡] Yohei Matsueda,[‡] Yasuhiro Oue,[‡] Kanji Komatsu,[‡] Keiichiro Imaizumi,[‡] Yuri Sakai,[‡] Satoshi Sugiura,[‡] Osami Takenouchi,[‡] Gen Unoki,^{*,‡} Yuko Yamakoshi,[‡] Vicky Cunliffe,[§] Julie Frearson,[§] Richard Gordon,[§] C. John Harris,[§] Heidi Kallou-Hosein,^{§,1} Joelle Le,^{§,#} Gita Patel,[§] Donald J. Simpson,[§] Brad Sherborne,^{§,∇} Peter S. Thomas,[§] Naotaka Suzuki,[‡] Midori Takimoto-Kamimura,[‡] and Ken-ichiro Kataoka[‡]

[‡]Teijin Institute for Bio-medical Research, Teijin Pharma Ltd., Hino, Tokyo 191-8512, Japan

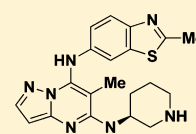
[§]BioFocus, Chesterford Research Park, Saffron Walden, Essex, CB10 1XL, U.K.

Supporting Information

ABSTRACT: A novel class of mitogen-activated protein kinase-activated protein kinase 2 (MAPKAP-K2) inhibitors was discovered through screening a kinase-focused library. A homology model of MAPKAP-K2 was generated and used to guide the initial SAR studies and to rationalize the observed selectivity over CDK2. An X-ray crystal structure of a compound from the active series bound to crystalline MAPKAP-K2 confirmed the predicted binding mode. This has enabled the discovery of a series of pyrazolo[1,5-*a*]pyrimidine derivatives showing good in vitro cellular potency as anti-TNF- α agents and in vivo efficacy in a mouse model of endotoxin shock.



(S)-44
MAPKAP-K2 : IC₅₀ = 0.13 μ M
CDK2 : IC₅₀ = 23 μ M



64
MAPKAP-K2 : IC₅₀ = 0.054 μ M
CDK2 : IC₅₀ 25 μ M

INTRODUCTION

Tumor necrosis factor- α (TNF- α) is implicated in several inflammatory diseases such as rheumatoid arthritis,¹ and biological agents such as infliximab, an anti-TNF- α antibody, have proved to be very effective medications for this disabling disease.^{2–5} Therefore, inhibition of TNF- α activity represents a most promising target for antiinflammatory therapy. The p38 mitogen-activated protein (MAP) kinase pathway has been shown to play an important role in the production of TNF- α and other cytokines.^{6,7} This pathway has therefore been of particular interest for the discovery of new antiinflammatory agents. Previous strategies to intervene in this pathway have been based largely on the development of selective inhibitors of p38 MAP kinase.⁸ Such inhibitors have proved to be effective inhibitors of proinflammatory cytokine production in cell-based assays and animal models of inflammatory disease. However, the p38 MAP kinase gene knockout mouse has proven to be embryonically lethal.^{9,10} Moreover, cells derived from such embryos have been demonstrated to have a number of abnormalities in fundamental cell responses. These observations may indicate that caution should be paid to long-term therapy with p38 MAP kinase inhibitors.¹¹

Given these caveats, an attractive alternative strategy for the development of antiinflammatory agents is the inhibition of this

pathway at the level of MAPKAP-K2. MAPKAP-K2 is a Ser/Thr kinase located downstream of p38 MAP kinase and is known to be a direct substrate of p38 MAP kinase.^{12–14} A role for MAPKAP-K2 in mediating the inflammatory response has been strongly implicated in the observed phenotype of the MAPKAP-K2-deficient mouse (MAPKAP-K2^{-/-}).^{13,15} This mutant mouse is viable and seems normal except for a significantly reduced inflammatory response. Mice deficient in MAPKAP-K2 produce less TNF- α and IL-6 than control littermates in response to lipopolysaccharide. In addition, MAPKAP-K2^{-/-} mice are protected against lipopolysaccharide-induced septic shock and collagen-induced arthritis.^{14–16} Their size, weight, and lifespan are similar to wild-type littermates when kept under germ-free conditions. In contrast to p38 MAP kinase, MAPKAP-K2 is not known to participate in feedback control loops that limit the production of proinflammatory cytokines or control the production of antiinflammatory cytokines.¹⁷

As a molecular mechanism to explain its involvement in inflammatory pathways, MAPKAP-K2 has been shown to directly regulate TNF- α by binding to AU-rich elements and

Received: July 5, 2011

Published: July 2, 2012

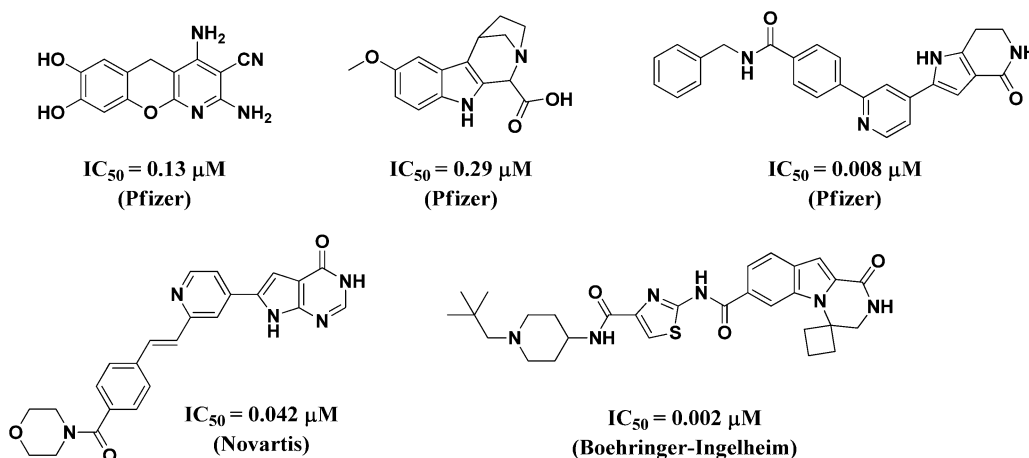


Figure 1. Reported MAPKAP-K2 inhibitors.

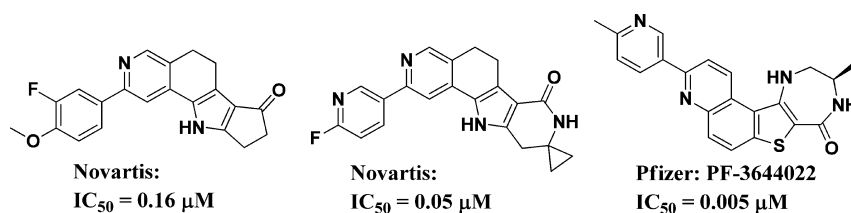


Figure 2. MAPKAP-K2 inhibitors demonstrating in vivo efficacy.

thereby affecting its RNA stability and/or translation.¹⁸ Therefore, MAPKAP-K2 could be a potentially more attractive target for antiinflammatory therapy than p38 MAP kinase.

The lack of clinical efficacy of all p38 MAP kinase inhibitors to date is most likely a result of biologic adaptation which results in the rapid reversal of early indications of benefit such as CRP levels.^{19,20} Because p38 MAP kinase is highly pleiotropic in its ability to intersect and regulate both proinflammatory and antiinflammatory pathways including JNK, MAP kinase phosphatase, IL-10, and negative feedback on TAK-1, there are multiple routes and mechanisms to allow for reversal of antiinflammatory effects. One could speculate that MAPKAP-K2, by the nature of its more downstream and less pathway convergent position in the network, could escape the majority of the compensatory mechanisms proposed for p38 MAP kinase inhibitors. This hypothesis however can only be proven by the development of well propertied molecules for clinical testing.

Several groups have subsequently reported programs also designed to develop antiinflammatory therapies through the generation of inhibitors of MAPKAP-K2.^{21–30} Example compounds illustrating the range of structure types reported as inhibitors of MAPKAP-K2 are shown in Figure 1.

Recent reports have detailed the in vivo activity of MAPKAP-K2 inhibitors, and three examples are shown in Figure 2. Novartis has reported compounds that inhibited LPS-induced TNF α release in mice and reduced paw swelling in a collagen-induced arthritis study in both rats and mice.^{31,32} Pfizer has reported oral antiinflammatory efficacy for PF-3644022 in both acute and chronic models of inflammation in rats.³³

At the inception of this project, there were no reported small molecule inhibitors of MAPKAP-K2 on which to initiate a program, and so it was decided to undertake a high-throughput screening campaign using a diverse set of 100 000 compounds. As this resulted in a very low hit rate, we next screened a focused kinase library³⁴ and identified a pyrazolo[1,5-*a*]pyrimidine

derivative (1), part of a small cluster of related hits that had modest inhibitory activity against MAPKAP-K2. In this paper, we report the discovery of this new class of MAPKAP-K2 inhibitors and describe the optimization of these pyrazolo [1,5-*a*] pyrimidine derivatives to produce potent and selective compounds.

RESULTS AND DISCUSSION

Screening against MAPKAP-K2 using a 100 000-member diverse library gave only a very low hit-rate of ATP-competitive compounds, and none of these were considered suitable for further development. Thus, a second campaign was conducted using a focused set of compounds designed to inhibit kinases;³⁴ 5075 compounds from 8 libraries, comprising 11 scaffold chemotypes, were used in this second screen, and 32 active compounds were identified and subjected to full IC₅₀ determinations. The active compounds were clustered around four distinct library scaffolds, and these clusters showed clear evidence of SAR. Representative compounds were subjected to kinetic determinations to ascertain their competitiveness with respect to ATP. The most promising hit compound based on its activity, kinetics, and the potential for follow up was the pyrazolo[1,5-*a*]pyrimidine 1.

The pyrazolo[1,5-*a*]pyrimidine 1 exhibited inhibition of MAPKAP-K2 (Figure 3), being marginally less potent than staurosporine (Figure 4) but clearly competitive with respect to ATP (Figure 5). The ATP concentrations of both the MAPKAP-K2 and CDK2 assays were set at the K_m value of MAPKAP-K2, i.e., at 10 μ M. In a focused panel of kinases, compound 1 was found to inhibit CDK2 more potently than MAPKAP-K2 and with either moderate or no activity against the other kinases screened (Figure 3). It was therefore decided to select CDK2 as a surrogate kinase for monitoring selectivity during the optimization of the hit compound. The observed activity against CDK2 was not unexpected given that the library SFK03 was designed to target the CDK family of kinases.

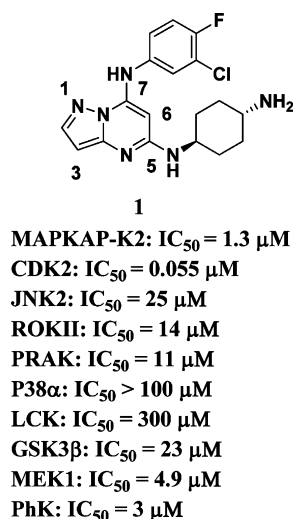


Figure 3. Structure and kinase selectivity of hit compound **1**.

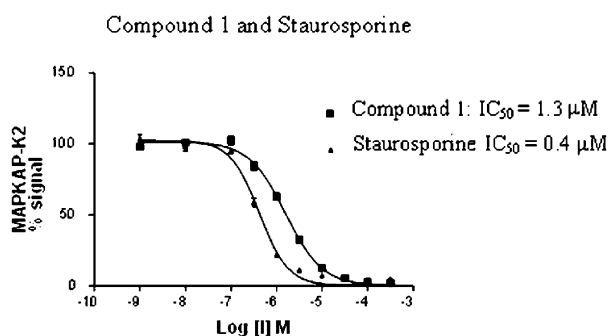


Figure 4. IC_{50} analysis of staurosporine and compound **1**. MAPKAP-K2 assay performed at $30 \mu M$ peptide, $10 \mu M$ ATP, $0.5 \mu Ci$ ^{33}P - γ -ATP/well for 10 min at room temperature. Data shown are mean \pm SEM of duplicate determinations.

Interference with the cell cycle via inhibition of cell cycle kinases is, in any event, likely to be an undesirable feature in antiinflammatory compounds.

Some minor modifications to the synthetic route used to prepare the initial hit library (SFK03) from which **1** emerged were undertaken to allow further substitution of this scaffold and the inclusion of a wider range of substituents. The preparation of the pyrazolo[1,5-*a*]pyrimidine derivatives described is outlined in Scheme 1. Synthesis began with the condensation of commercially available 3-aminopyrazole (**2**) and various malonate derivatives to construct the pyrazolo[1,5-*a*]pyrimidine core. The resulting dihydroxy derivative **3** was converted to 5,7-dichloropyrazolo[1,5-*a*]pyrimidine (**4**) by treatment with phosphorus oxychloride. For the syntheses of the 3-halogenated compounds, the halogen was introduced at this stage using *N*-chlorosuccinimide or *N*-bromosuccinimide (Scheme 2). Selective introduction of various anilines at the 7-position to give **5** was achieved by heating with the respective anilines in the presence of base. Following Boc protection to give **6**, the subsequent introduction of amines at the 5-position was achieved by heating with an excess of the amine **7**. For the syntheses of the ether-linked derivatives at the 5-position, the alcohol derivative **10** was introduced as the alkoxide (generated from the alcohol and sodium hydride). Finally, deprotection of the Boc-protected compounds (**8** and **11**) gave the target compounds **9** and **12**. For further transformations of the

substituents at the 7-position, condensation or coupling reactions were carried out before removal of the Boc groups as shown in Schemes 3–5. This route was successfully applied to a variety of 3-, 5-, and 7- substituted pyrazolo[1,5-*a*]pyrimidines.

Despite the 24-fold inverse selectivity with respect to CDK2, and given the very low screening hit-rate for MAPKAP-K2, compound **1** was considered to offer promising scope for optimization. An evaluation of the ADME properties of compound **1** showed the compound to have good properties and to be a suitable scaffold on which to undertake an optimization program. To facilitate the medicinal chemistry efforts, it was considered important to predict the likely binding modes of compound **1** to MAPKAP-K2 and CDK2. However, at this stage a crystal structure of MAPKAP-K2 was not available and it was therefore necessary to build a homology model of MAPKAP-K2 to enable docking studies to be carried out.

A homology model of MAPKAP-K2 was constructed based on the reported X-ray structures of phosphorylase kinase³⁵ and cAMP-dependent protein kinase,³⁶ each of which show ca. 30% sequence identity with MAPKAP-K2 using the Biopolymer Composer module in Sybyl, v6.8.³⁷ As the central scaffold of compound **1** is structurally very similar to purvalanol B, a known inhibitor of CDK2 (Figure 6), compound **1** was docked in the MAPKAP-K2 model such that the overall geometry was as close as possible to that of purvalanol B in CDK2.³⁸ In the resulting docking mode, compound **1** appeared to form hydrogen bonds with the main chain NH and C=O groups of Leu¹⁴¹ in the hinge region, and the terminal positively charged amine of the *trans*-4-aminocyclohexylamino side chain was able to form a hydrogen bond to Asn¹⁹¹ and a salt bridge to Asp²⁰⁷, as shown in Figure 7.

As expected, the predicted binding mode of compound **1** with MAPKAP-K2 was very similar to that seen with CDK2. However, the detailed differences in the residues within the ATP-binding site of the two kinases suggested that the required MAPKAP-K2 selectivity might be achieved by varying the side chains while seeking to retain this overall binding mode. We therefore embarked on a detailed SAR study of a series of pyrazolo[1,5-*a*]pyrimidine analogues to identify the key functionality responsible for activity against MAPKAP-K2 and selectivity over CDK2.

Initial investigations of the effect of 2-position substitution of the scaffold were carried out to test the predicted binding mode of compound **1** with MAPKAP-K2. This mode suggested that there was little available space to accommodate substituents in this position, as there would be a steric clash with the ATP-site backbone. Indeed, it was found that the introduction of substituents at this position resulted in significant losses in potency against MAPKAP-K2 (Table 1: compounds **20** and **21**).

The binding mode of compound **1** suggested that substitution at the 3-position would offer a means of accessing the hydrophobic subpocket of the ATP site. We considered that suitable substituents at this position might lead both to an improvement of MAPKAP-K2 activity and selectivity over other kinases, based on the variability of the shape of the hydrophobic subpocket compared with other more conserved regions of the active site. However, all 3-substituted analogues prepared in this study resulted in a reduction of activity against MAPKAP-K2 (Table 1: compounds **22**–**24**). These results suggested that the hydrophobic subpocket in MAPKAP-K2 was too small to accommodate any substituent at this position of the ligand. Moreover, contrary to our expectations, we found that compounds with halogens (Cl, Br) or a cyano group at this

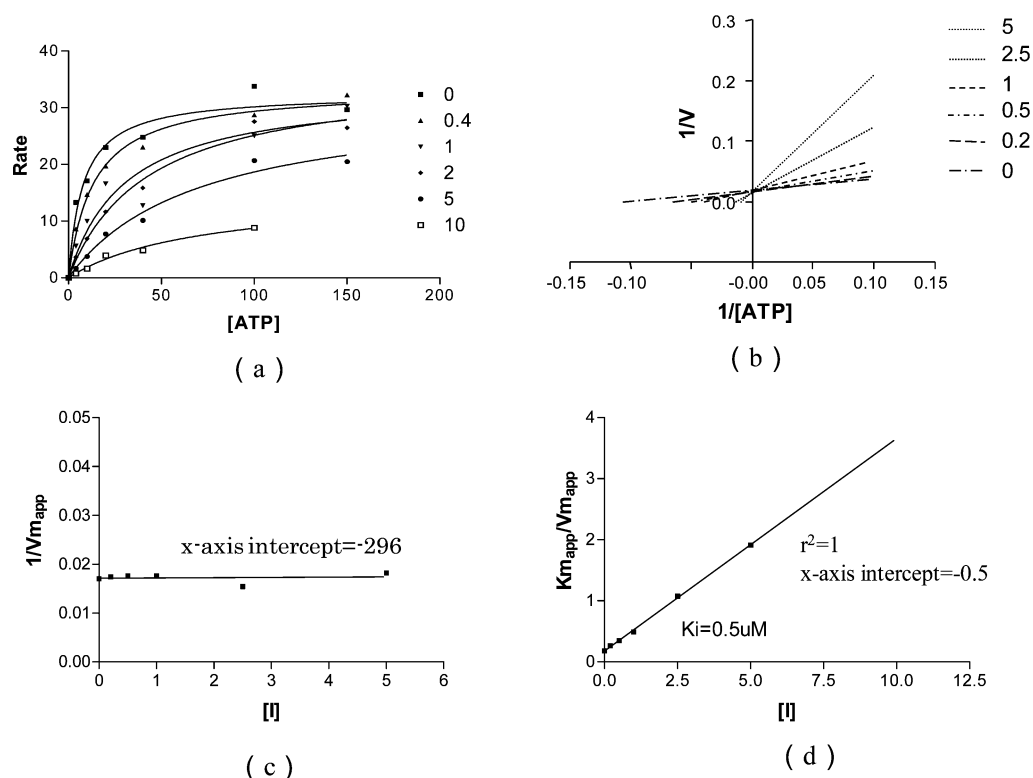
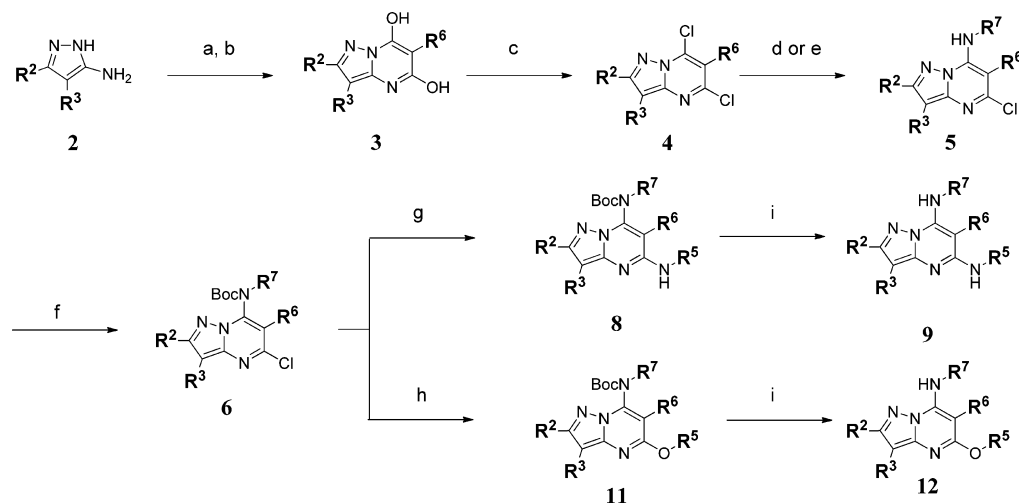


Figure 5. Mechanism of action/ K_i determination for compound 1. (a) Primary plot: Rate vs [ATP]. (b) Secondary Lineweaver–Burke plot of $1/V$ vs $1/[ATP]$. (c) Secondary plot of $1/V_{m_{app}}$ vs [I]. (d) Secondary plot of $K_{m_{app}}/V_{m_{app}}$ vs [I]. MAPKAP-K2 assay was performed at $30\ \mu\text{M}$ peptide under a matrix range of concentrations of ATP ($4\text{--}150\ \mu\text{M}$) and compound ($0\text{--}20\ \mu\text{M}$) in the presence of $1\ \mu\text{Ci}\ ^{33}\text{P}\text{-}\gamma\text{-ATP}$ /well for 10 min. Reaction rates are expressed as femtomoles of peptide phosphorylated per minute per μM MAPKAP-K2. Data shown are mean of duplicate data points; experiments were conducted across three independent determinations yielding K_i values of $7\ \mu\text{M}$, $7\ \mu\text{M}$, and $6\ \mu\text{M}$, respectively.

Scheme 1. General Synthetic Route^a



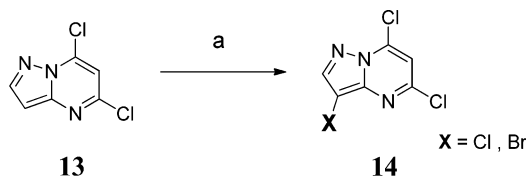
^aReagents and conditions: (a) $\text{R}^6\text{-CH}(\text{COOEt})_2$, EtONa, EtOH, reflux; (b) HCl aq; (c) POCl_3 , Me_2NPh , reflux; (d) $\text{H}_2\text{N-R}^7$, Et_3N , tPrOH , reflux; (e) $\text{H}_2\text{N-R}^7$, NaH, DMF/THF, room temp to $-50\ ^\circ\text{C}$; (f) Boc_2O , DMAP (cat.), 1,4-dioxane, room temp; (g) excess $\text{H}_2\text{N-R}^5$ (7), $90\ ^\circ\text{C}$; (h) HO-R^5 (10), NaH, THF, $0\ ^\circ\text{C}$ to room temp; (i) TFA, CH_2Cl_2 , room temp.

position showed more potent inhibitory activity against CDK2. Recently we have confirmed that a cyano group at the 3-position of such ligands interacts with the phenyl ring of the Phe⁸⁰ gatekeeper residue of CDK2 by solving the crystal structure of compound 22 in complex with CDK2 (unpublished data). Our observations of the improved potency against

CDK2 with substituents at this position are consistent with the data published by other groups,³⁹ whereby 3-substituents such as CN, tPr , and Br improve potency against CDK2.

A significant breakthrough in selectivity for MAPKAP-K2 over CDK2 was achieved when substituents were introduced at the 6-position. As seen in Table 2, the addition of a small alkyl group

Scheme 2



Reagents and conditions: (a) *N*-chlorosuccinimide or *N*-bromosuccinimide, CHCl_3 , room temp.

at the 6-position led to a dramatic drop in potency against CDK2 even though the inhibitory activity against MAPKAP-K2 was significantly increased.

Although a range of smaller substituents at the 6-position are tolerated, increased steric bulk at this position led to a progressive reduction of the inhibitory activity against MAPKAP-K2. In conclusion, small alkyl groups such as methyl or ethyl were found to be preferred.

Encouraged by the beneficial effects of substitution at the 6-position, we investigated the importance of the *trans*-4-aminocyclohexylamino group at the 5-position. It was found that the presence of the terminal amino group and its orientation and distance from the scaffold were very critical for potency; in particular, retaining the postulated salt bridge to Asp²⁰⁷ seemed to be critical. Replacement of the linking -NH- group with the -O- group was well tolerated (Table 3: compound 47). In summary, replacement of the *trans*-4-aminocyclohexylamino group with the (\pm)-3-piperidylamino group resulted in similar levels of potency (Table 3: compound 38 vs compound 44) or a modest improvement in potency (Table 3: compound 35 vs compound 1).

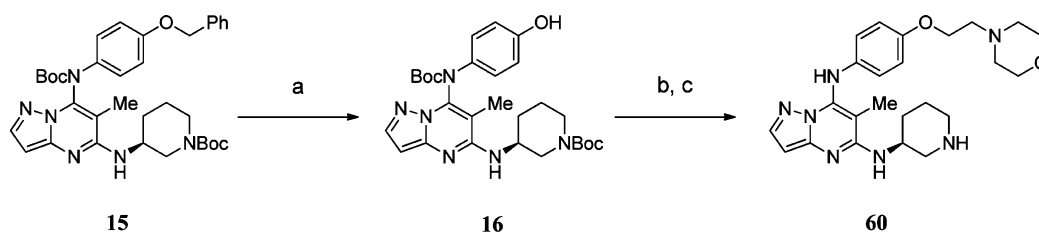
We subsequently showed that a methyl group at the 6-position in combination with the (\pm)-3-piperidylamino group at the 5-position was preferred over the ethyl or unsubstituted analogues. As shown in Table 4, compound 48 showed MAPKAP-K2 inhibition with an IC_{50} of 0.51 μM and, more importantly, improved selectivity over CDK2 compared to the other compounds (35 and 49). Finally, for compound 44, we showed that the (*S*)-enantiomer of the 3-piperidylamino group exhibited better potency than the (*R*)-enantiomer at the 5-position (Figure 8). An increase in MAPKAP-K2 potency of up to 10-fold was achieved by the initial derivatization of the 5-, 6-, and 7-position substituents in compound 1 to provide (*S*)-44. The compounds with a 3-piperidylamino group at the 5-position were observed to have better selectivity against CDK-2 compared to those with a 4-aminocyclohexylamino group (compound 35 vs 1 and compound 48 vs 25). As a result of this improved selectivity, the 3-piperidylamino group was selected as the preferred 5-position substituent for further optimization studies.

Following up on these findings, we undertook a further round of optimization of the substituents at the 7-position. According to the predicted binding mode, it appeared that the NH group in this position is involved in hydrogen bonding to the carbonyl group of Leu141. Indeed, it was found that methylation of the 7-position NH group led to a complete loss in potency, which supports the involvement of this group in a key binding interaction (Table 5: compound 50). Replacing a phenyl group in the 7-position by alkyl or benzyl groups led to a significant loss of potency (Table 5: compounds 51–53), indicating the necessity for an aromatic ring at the 7-position. The SAR of the 7-aryl group was explored to further increase the activity against MAPKAP-K2. A positional scan of the substituents on the 7-phenyl group indicated that para-substitution was preferred and that a relatively large substituent, whether electron-withdrawing (compound 54) or electron-donating (compound 55) was tolerated. This is consistent with the predicted binding mode which indicated that substituents at the para-position of the phenyl group would be directed toward the external surface out of the ATP binding site. Taking this into account, we synthesized further analogues possessing hydrophilic groups in the para-position but little improvement was achieved (Table 6, compounds 59 and 60).

At this stage, we succeeded in solving the X-ray cocrystal structure of the complex of (*S*)-44 with MAPKAP-K2⁴⁰ and confirmed that the binding mode predicted from the homology model was essentially correct. However, as a result of a conformational change in the flexible glycine-rich loop (aka P-loop), the hydrophobic site in the region adjacent to the ligand was somewhat larger than was previously predicted. On the basis of this observation from the X-ray crystal structure, we synthesized further derivatives intended to pick up additional hydrogen bond interactions within this site. It was found to be difficult to improve the potency dramatically by the introduction of hydrogen bond donors and acceptors in the 7-position substituent. This is likely to be a consequence of the site being not just a hydrophobic site but also being exposed to the solvent surface. Analogues with bicyclic heteroaryl or biaryl groups in the 7-position were designed to expand the contact surface with this hydrophobic site (Table 6). We were thus able to identify compound 64 as the most potent analogue in our series, and this compound showed a MAPKAP-K2 inhibition activity of less than 100 nM with greater than 400-fold selectivity over CDK2.

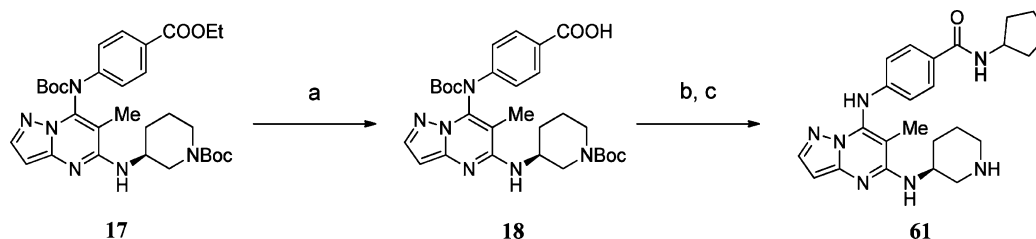
As indicated above, we solved the X-ray cocrystal structure of the complex of (*S*)-44 with MAPKAP-K2 at 2.9 Å resolution⁴⁰ (PDB ID 3A2C). MAPKAP-K2: (*S*)-44 crystals belonged to the space group of $P2_12_12_1$, and there were 12 molecules in each asymmetric unit. Surprisingly, it was found that each

Scheme 3



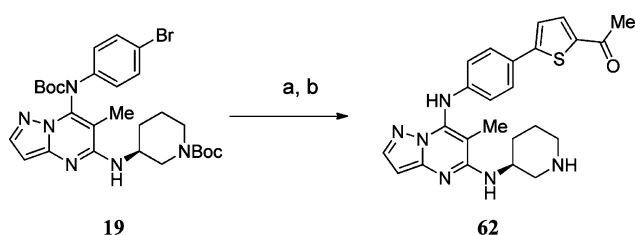
Reagents and conditions: (a) $\text{Pd}(\text{OH})_2/\text{C}$, H_2 , MeOH; (b) 2-methoxyethanol, PPh_3 , diisopropyl azodicarboxylate in toluene, THF, room temp; (c) TFA, CH_2Cl_2 , room temp.

Scheme 4



Reagents and conditions: (a) NaOH aq, MeOH, room temp then HCl aq; (b) carbonyldiimidazole, cyclopentylamine, DMF, room temp; (c) TFA, CH₂Cl₂, room temp.

Scheme 5



Reagents and conditions: (a) 5-acetyl-2-thiopheneboronic acid, Pd(OAc)₂, Na₂CO₃, PPh₃, 1,4-dioxane/H₂O; (b) TFA, CH₂Cl₂, room temp.

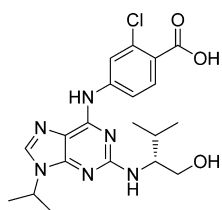


Figure 6. Structure of purvalanol B.

enzyme complex bound two molecules of (*S*)-44. One molecule of (*S*)-44 was bound to the ATP-binding site between the N-terminal and C-terminal domains as expected, and the other molecule of (*S*)-44 was bound near the substrate-binding site of the C-terminal domain as shown in Figure 9. Although there were two (*S*)-44 molecules in each complex,

Table 1. IC₅₀ Values for 2- or 3-Position Derivatives

compd	R ²	R ³	MAPKAP-K2 IC ₅₀ (μM)	CDK2 IC ₅₀ (μM)	selectivity CDK2/ MAPKAP-K2
1	H	H	1.3	0.055	0.042
20	Me	H	>300	–	–
21	^t Bu	H	>300	–	–
22	H	CN	3.1	0.0040	0.0013
23	H	Cl	8.1	0.0030	0.0004
24	H	Br	9.2	0.0034	0.0004

the (*S*)-44 molecule bound to the ATP-binding site is presumably the key interaction for the MAPKAP-K2 inhibitory activity as the analogous pyrazolo[1,5-*a*]pyrimidine derivative **1** exhibited clear ATP-competitive inhibitory activity. On the other hand, an assay to examine substrate competitiveness failed to detect any binding of (*S*)-44 in the substrate binding pocket. Therefore, the binding of (*S*)-44 near the substrate-binding site is very weak and does not appear to contribute to the inhibitory activity against MAPKAP-K2. Interestingly, two recent reports indicate similar behavior in p38α MAP kinase, where lipid ligands⁴¹ or small-molecule p38α inhibitors⁴² bind to the C-terminal cap region formed from the conserved MAP kinase insert, in the latter case in

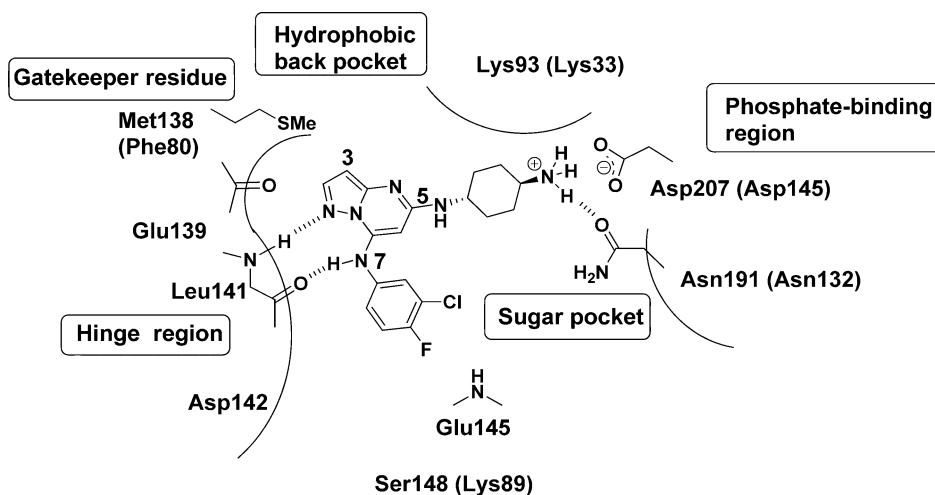
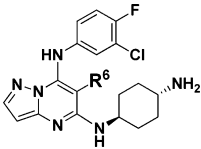


Figure 7. Predicted binding mode of compound (**1**) in the MAPKAP-K2 homology model. Equivalent residue numbers in CDK2 are shown in parentheses.

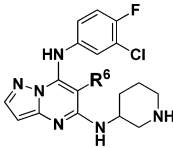
Table 2. IC₅₀ Values for 6-Position Derivatives


compd	R ⁶	MAPKAP-K2 IC ₅₀ (μM)	CDK2 IC ₅₀ (μM)	selectivity CDK2/ MAPKAP-K2
1	H	1.3	0.055	0.042
25	Me	0.40	11	27
26	Et	0.40	3.6	9.0
27	ⁿ Pr	0.6	2.1	3.5
28	Ph	1.6	6.0	3.8

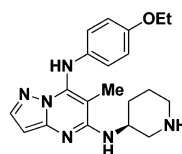
addition to the ATP site as seen in this work; the binding affinity at this second site is suggested to be greater than observed herein for MAPKAP K2.⁴²

We were able to use the binding mode of (*S*)-44 in the ATP-binding site to rationalize the previously observed SAR of this series of analogues. A schematic representation of the observed interactions is shown in Figure 10, these being largely consistent with those predicted from the homology model.

Compound (*S*)-44 makes two hydrogen bonds with the main chain NH and carbonyl oxygen of Leu¹⁴¹ at the hinge region as expected. The charged amino group of the 5-(3*S*)-piperidyl moiety forms a salt bridge with the side-chain carboxyl group of

Table 4. IC₅₀ Values for 6-Position Derivatives with (*rac*)-3-Piperidylamino Group at the 5-Position


compd	R ⁶	MAPKAP-K2 IC ₅₀ (μM)	CDK2 IC ₅₀ (μM)	selectivity CDK2/ MAPKAP-K2
35	H	0.40	0.70	1.8
48	Me	0.51	33	65
49	Et	0.70	24	34

(*S*)-44MAPKAP-K2 : IC₅₀ = 0.13 μMCDK2 : IC₅₀ = 23 μM

Selectivity (CDK2/MAPKAP-K2) : 177

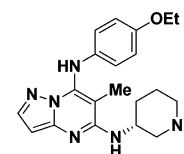
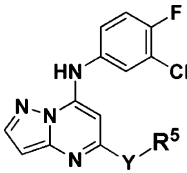
(*R*)-44MAPKAP-K2 : IC₅₀ = 1.2 μMCDK2 : IC₅₀ > 100 μM

Figure 8. Determination of preferred enantiomer.

Table 3. IC₅₀ Values for 5-Position Derivatives


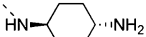

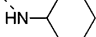
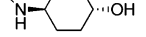
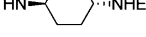

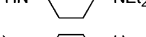

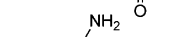

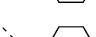
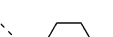
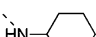
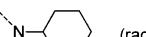
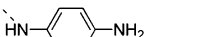
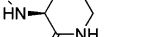
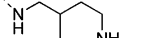
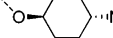

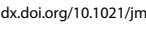
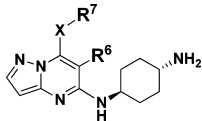
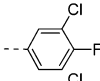
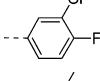
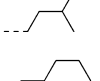
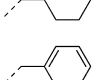
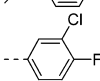
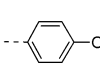
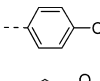
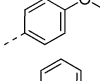
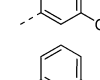
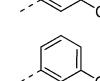
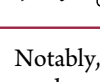
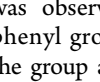
compd	--Y-R ⁵	MAPKAP-K2 IC ₅₀ (μM)	compd	--Y-R ⁵	MAPKAP-K2 IC ₅₀ (μM)
1		1.3	38		0.36
29		>100	39		89
30		2.0	40		2.5
31		>100	41		8.7
32		>100	42		4.1
33		>100	43		83
34		25	44		0.40
35		0.40	45		26
36		>100	46		>100
37		>100	47		0.57

Table 5. IC₅₀ Values for 7-Position Derivatives


compd	--R ⁶	--X	--R ⁷	MAPKAP-K2 IC ₅₀ (μM)
1	--H	--NH		1.3
50	--H	--N(Me)		>300
51	--H	--NH		12
52	--H	--NH		11
53	--H	--NH		7.0
25	--Me	--NH		0.40
38	--Me	--NH		0.36
54	--Me	--NH		0.70
55	--Me	--NH		0.70
56	--Me	--NH		1.4
57	--Me	--NH		1.9
58	--Me	--NH		3.0

Asp²⁰⁷ together with bidentate hydrogen bonds to the main chain carbonyl oxygen of Glu¹⁹⁰ (2.84 Å) and the carbonyl oxygen on the side chain of Asn¹⁹¹ (3.10 Å). The other significant interaction is the van der Waals contact between the 7-*p*-ethoxyphenyl group and the sulfur atom of Cys¹⁴⁰. According to this X-ray cocrystal structure, there is little available space around the 3-position, and this is consistent with the SAR observations at this position.

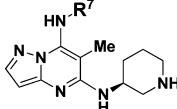
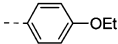
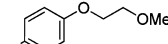
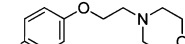
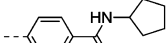
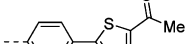
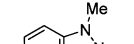
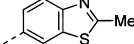
The cocrystal structure of MAPKAP-K2 and (S)-44 also provided useful information for understanding the improvement of selectivity for MAPKAP-K2 over CDK2. We found that the Gly-rich loop took the α -helical conformation (α -form), while other reported MAPKAP-K2 complexes with ADP, staurosporine, or various small molecule inhibitors showed the Gly-rich loop in a β -sheet conformation (β -form). As can be seen in Figure 11, it was found that the α -form had a slightly larger hydrophobic site compared to that of the β -form around the 7-position substituents. (S)-44 exhibits a nonplanar conformation due to the repulsion of the 7-substituent and the methyl group at the 6-position, and this feature distinguishes it from other MAPKAP-K2 inhibitors. The interaction with the nonplanar form of (S)-44 induces the secondary structural change of the Gly-rich loop from a β -sheet form to the α -helical form to avoid the conflict of the substituent at the 7-position with Leu⁷⁰. As a result of this structural change, a new pocket composed of Asp¹⁴², Cys¹⁴⁰, Gln⁸⁰, and Leu⁷⁹ emerged and the *p*-ethoxyphenyl group at the 7-position of (S)-44 bound in this new pocket.

Notably, a significant improvement in selectivity over CDK2 was observed in the compounds with an ortho-substituted phenyl group at the 7-position; this trend became greater as the group at the 6-position became larger (Table 7). The combined effect of these two substituents is to reinforce the nonplanarity of the 7-substituent and, owing to the larger hydrophobic pocket in MAPKAP-K2 compared to CDK2, this leads to an additive effect in terms of selectivity; however, the MAPKAP-K2 potency of these analogues was generally reduced.

Recently, a structure of a CDK2-(S)-44 complex was obtained in our laboratory. It was observed that the Gly-rich loop of CDK2 adopted the β -sheet conformation, with (S)-44 taking a distorted planar conformation to avoid a clash of the 7-substituent with the Gly-rich loop as anticipated. Moreover, the 3-piperidylamino group at the 5-position did not make a favorable interaction similar to that observed in the MAPKAP-K2:(S)-44 complex between the charged amino group and Asp²⁰⁷, Glu¹⁹⁰, and Asn¹⁹¹ as shown in Figure 10.⁴³

The kinase selectivity of (S)-44 was evaluated in a single point assay at 10 μ M against more than 100 kinases (Supporting Information Table S1). The majority of kinases (95) were inhibited by less than 30% at this concentration. Five kinases were inhibited by >75%, MAPKAP-K2, CHK2, Yes, Fes, and Flt3, with MAPKAP-K2 showing the highest levels of inhibition. The inhibition data against a subset of related kinases are summarized in Table 8. It was observed that (S)-44

Table 6. IC₅₀ Values for 7-Position Derivatives

compd	--R ⁷			
		MAPKAP-K2 IC ₅₀ (μM)	CDK2 IC ₅₀ (μM)	selectivity CDK2/MAPKAP-K2
(S)-44		0.13	23	177
59		0.13	22	169
60		0.16	62	388
61		0.14	49	350
62		0.057	21	368
63		0.076	27	355
64		0.054	25	463

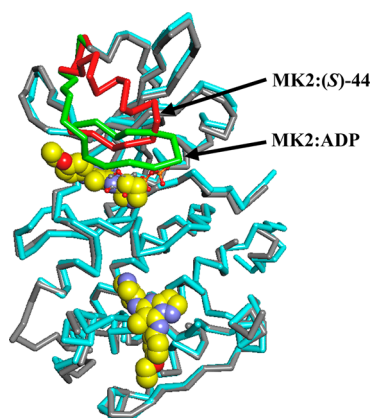


Figure 9. Overlay of crystal structure of MAPKAP-K2 with (S)-44 (gray and red) and MAPKAP-K2 with ADP (blue and green). There are two molecules of (S)-44 in each monomer complex. One molecule of (S)-44 was bound to the ATP-binding site between the N-terminal and C-terminal domains, and the other molecule of (S)-44 was bound near the substrate-binding site of the C-terminal domain. The Gly-rich loop of MAPKAP-K2 with (S)-44 took the α -helix conformation (α -form: shown in red), while MAPKAP-K2 with ADP showed the Gly-rich loop in a β -sheet conformation (β -form: shown in green).

exhibited very good levels of selectivity over this set of related kinases. Three of the kinases inhibited modestly by the initial hit compound **1**, i.e., MEK1, PRAK, and ROKII (Figure 3), were not inhibited to any significant extent by (S)-44.

The initial profiling round indicated that (S)-44 had significant inhibitory activity (IC₅₀ 1.7 μM) toward CHK2 using a radiometric assay. The screening of further analogues (compounds **26**, **38**, and **65**) and the use of an orthogonal assay platform confirmed that these compounds showed no

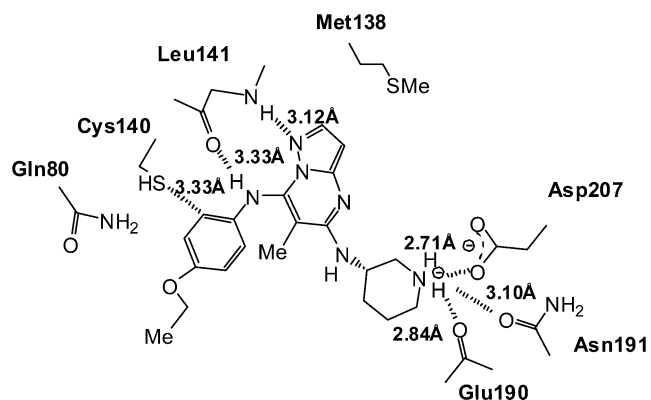


Figure 10. The binding interaction of compound (S)-44 and MAPKAP-K2.

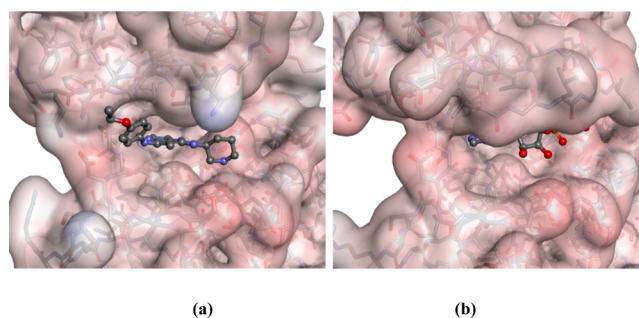
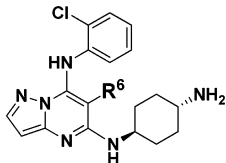


Figure 11. The ATP-binding pocket of (a) MAPKAP-K2 with (S)-44 (α -form) PDB ID 3A2C and (b) MAPKAP-K2 with ADP (β -form) (PDB ID 1NY3) viewed from the same angle.

inhibition of CHK2 at 30 μM. While we were unable to determine the reason for the different activities demonstrated

Table 7. IC₅₀ Values for 7-Position Ortho-Substituted Derivatives


compd	R ⁶	MAPKAP-K2 IC ₅₀ (μM)	CDK2 IC ₅₀ (μM)	selectivity CDK2/ MAPKAP-K2
65	H	0.2	0.39	2
66	Me	1.7	6.4	3.8
67	Et	1.5	>300	>200

Table 8. Kinase Selectivity of Compound (S)-44^a

kinase	inhibition (%)	kinase	inhibition (%)
CDK1/cyclinB(h)	12	AMPK(r)	35
CDK2/cyclinE(h)	13	CaMK2(r)	41
ERK2(h)	7	CaMK4(h)	-38
IKKβ(h)	7	CHK1(h)	30
JNK1α1(h)	0	PKBα(h)	3
JNK2α2(h)	-33	p70S6K(h)	-1
p38α(h)	4	PDK1(h)	-9
p38β(h)	-14	PKA(h)	0
p38γ(h)	-2	PKCα(h)	5
p38δ(h)	3	PKCγ(h)	-5
MKK4(m)	15	ROCK-II(h)	23
MKK6 (h)	24	Rsk2(h)	9
MKK7β(h)	26	PRAK(h)	62
MEK1(h)	19		

^a10 μM, single-point assay; (h) = human, (m) = mouse, (r) = rat. Inhibition of CHK2 by (S)-44 was measured using a Cyclex assay (IC₅₀ >30 μM).

by (S)-44 in the two assay formats, we concluded that the series was not significantly active against CHK2.

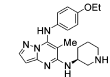
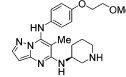
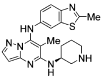
In addition to demonstrating excellent selectivity over a panel of kinases, the series retained the good ADME properties of the initial hit compound **1** (i.e., high stability in human and mouse liver microsomes, good permeability in Caco-2 cells). A comparison of some ADME properties for **1** and (S)-44 are shown in Table 9.

Table 9. ADME Properties for **1** and (S)-44

	1	(S)-44
solubility pH 7.4 (μg/mL)	75	70
human microsomes (CL _{int} μL/min/mg)	<10	<10
mouse microsomes (CL _{int} μL/min/mg)	59	11
Caco-2 permeability (Papp A to B × 10 ⁻⁶ cm/s)	7.1	28.3
mouse PPB (fraction bound)	-	88.6%

Compounds (S)-44, **59**, and **64** were further tested in a cellular assay that measures LPS-stimulated TNF-α production from THP-1 cells (human acute monocytic leukemia cell line) and demonstrated good in vitro cellular potency as anti-TNF-α agents with no cytotoxic effects evident (Table 10) (see Supporting Information Figures S1–3). (S)-44 also demonstrated inhibition of LPS-stimulated TNF-α production in human and mouse whole blood assays. The observed drop-off in potency between the enzymatic assay and the cell-based or

Table 10. In Vitro Cellular Potency and Pharmacokinetic Profile^a

Compound	(S)-44	59	64
Structure			
MAPKAP-K2 IC ₅₀ (μM)	0.13	0.13	0.054
Cellular potency IC ₅₀ (μM) (THP-1 cell)			
TNF-α	7.2	7.6	8.4
Cell viability IC ₅₀ (μM)			
MTS	74	>100	54
Whole blood assay ^b IC ₅₀ (μM)			
TNF-α	11 (human) 5 (mouse)	-	-
Mouse PK Profile (1mg/kg)			
Bioavailability (%F)	66	80	79
AUC 0-24, (nM.hr) p.o.	438	316	579
CL tot (L/hr/kg)	4.1	3.5	3.5
T _{1/2} i.v. (hr)	2.2	1.0	2.6

^aDose: 1 mg/kg iv (0.5% Tween 80 in saline) and 1 mg/kg po (0.5% methyl cellulose) in male mice (three mice per group). ^bFour-fold diluted blood was used.

whole blood assays is typical of that seen in other similar programmes and can be attributed to the higher ATP concentration in the cells (typically 1–10 mM) compared to that in the enzymatic assay system (ATP concentration = 10 μM). It was also confirmed by Western blot (Figure 12) that HSP27,

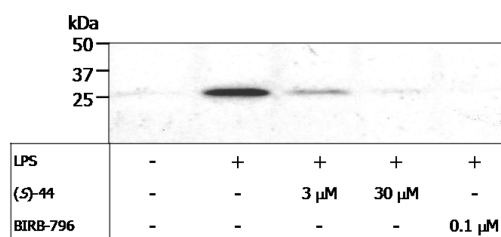


Figure 12. (S)-44 inhibits LPS-induced phosphorylation of HSP27 in cells. THP-1 cells were preincubated with vehicle or test compound prior to addition of LPS (10 μg/mL). Cell lysates were subjected to SDS-PAGE analysis (equivalent protein load in each lane: 20 μg) and transferred proteins subjected to immunoblotting with an antiphospho HSP27 antibody.

the downstream substrate of MAPKAP-K2, was inhibited in THP-1 cells treated with (S)-44 at 3 and 30 μM. These data are primarily qualitative but do show indications of a concentration-related effect of (S)-44 and provide evidence that this compound was most likely acting 'on-target' on MAPKAP-K2 in cells. The pharmacokinetic properties of these compounds were also evaluated in mice and showed good absorption after oral administration (Table 10).

Compound (S)-44 was used to evaluate the effect of MAPKAP-K2 inhibitors on the in vivo serum concentration of TNF-α in a murine model of endotoxin shock. Vehicle (5 mM HCl/saline) or compound (S)-44 at each dose (mg/kg body weight) was administered orally into C57BL/6 mice (200 μL/mouse). LPS (0.5 mg/kg) was administered

intraperitoneally 30 min after the compound was injected. Sixty minutes after the LPS injection, blood was collected through the abdominal vein under barbiturate anesthesia. Serum was collected, and the TNF- α concentration was measured by an ELISA method. A dose-dependent decrease in serum TNF- α concentration was observed in the mice treated with (S)-44 and was similar to the response seen with BIRB 796 as standard (Figure 13). In the mice dosed orally at 100 mg (S)-44/kg

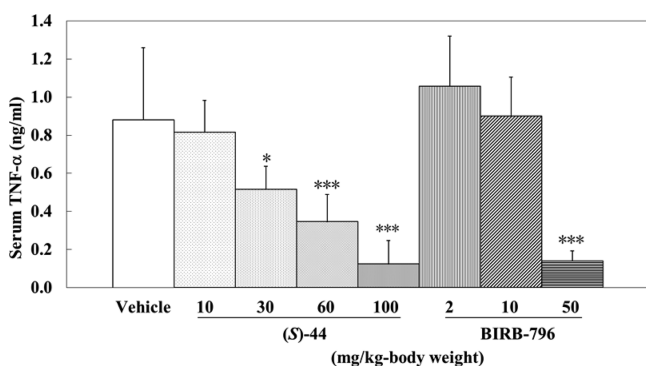


Figure 13. The effect of compound (S)-44 on serum TNF- α concentration in mouse endotoxin shock model. Statistical analysis was carried out with the Dunnett's multiple comparison test, with $P < 0.05$ considered as significant. * $P < 0.05$ and *** $P < 0.001$ (vs control).

body weight, the level of serum TNF- α was approximately 14% compared with that of the vehicle-administered group. The serum concentration of compound in the (S)-44-administered group dose-dependently increased from 2, 5, 8, to 10 μM following dosing at 10, 30, 60, and 100 mg/kg (Figure 12), these concentrations being comparable to the IC_{50} values obtained in the whole blood assay (mouse: $\text{IC}_{50} = 5 \mu\text{M}$). We conclude that orally administered (S)-44 was absorbed and was able to reach the concentrations necessary to effectively inhibit TNF- α production in a manner similar to that observed in the whole blood assay. Considering both the observed kinase selectivity profile of (S)-44 and the observed repression of HSP27 phosphorylation in the cell-based assay, the inhibition of MAPKAP-K2 activity contributed to a decrease in the concentration of serum TNF- α . Further results of detailed preclinical studies will be disclosed in a forthcoming publication.

CONCLUSIONS

We have demonstrated that novel pyrazolo[1,5-*a*]pyrimidine compounds are useful as MAPKAP-K2 inhibitors. SAR studies were conducted to optimize this series of pyrazolo[1,5-*a*]pyrimidine analogues, resulting in the identification of the highly potent and selective compound 64. The MAPKAP-K2 inhibitory activity of 64 was increased by more than 20-fold over 1, and selectivity over CDK2 was improved by more than 10 000-fold. According to the structural analysis of the MAPKAP-K2/(S)-44 complex, the effect of the 6-substituent on the improvement of selectivity over CDK2 can be rationalized. Members of the pyrazolo[1,5-*a*]pyrimidine series exhibited good in vitro cellular potency in LPS-induced TNF- α secretion cell models and a favorable PK profile. Furthermore, we have also demonstrated the efficacy of (S)-44 in reducing TNF- α production in the murine endotoxin shock model. The excellent in vitro kinase selectivity of (S)-44 (see Supporting Information Table S1) plus its demonstrated inhibition of HSP27 phosphorylation, a direct substrate of MAPKAP-K2,

provides confidence that this compound elicits its effect on TNF- α secretion through inhibition of MAPKAP-K2.

EXPERIMENTAL SECTION

Commercial chemicals and solvents were of reagent grade and used without further purification. Reactions sensitive to moisture or air were performed under nitrogen using anhydrous solvents and reagents. The progress of reactions was determined by either analytical thin layer chromatography (TLC), performed with TLC Silica gel 60 F254, or liquid chromatography–mass spectrometry (LC-MS). Silica gel column chromatography was performed with the indicated solvent and using silica gel 60. Chemical yields are not optimized. The purity of all compounds screened in biological assays was determined to be >95% by HPLC/MS analysis. NMR experiments were recorded on a 400 MHz machine and are referenced to residual solvent signals: CDCl_3 (δ 7.26) or $\text{DMSO}-d_6$ (δ 2.49). Chemical shifts are reported in δ units (parts per million) and are assigned as singlet (s), doublet (d), doublet of doublets (dd), triplet (t), multiplet (m), broad signal (br), or very broad signal (vbr). Coupling constants (J) are reported in hertz (Hz). High-resolution mass spectrometry (HRMS) measurement was performed on a LCMS-IT-TOF.

General Procedure A for the Synthesis of Compound 3. To a stirred solution of sodium ethoxide (50 mmol) in EtOH (100 mL) were added the appropriately 2-substituted malonic acid diester (20 mmol) and appropriately substituted 3-aminopyrazole (20 mmol). The mixture was heated at reflux for 18 h, during which a precipitate was formed. (In several cases where the substituent was an alkyl chain, little or no precipitate was formed. In these situations, EtOH was removed under reduced pressure. The residue was partitioned between water and EtOAc, and the phases were separated. The aqueous phase was acidified (pH 2) with 12 N HCl and back-extracted with EtOAc ($\times 2$). The organic phase was washed with water and brine, dried over anhydrous Na_2SO_4 , and concentrated to give crude compound 3.) The reaction mixture was cooled to room temperature, and the precipitate was collected by filtration and washed with EtOH. The solid was dried under vacuum. The dried solid was dissolved in water (100 mL), and the resulting solution was acidified at pH 2 with 12 N HCl. The solid was collected by filtration and washed with water to give a crude compound 3. This crude product was used in the next reaction without further purification.

General Procedure B for the Synthesis of Compound 4. The crude compound 3 (10 mmol) was dissolved in phosphorus oxychloride (20 mL), and *N,N*-dimethylaniline (1.0 mL) was added. The mixture was heated at reflux for 18 h. Excess phosphorus oxychloride was removed in vacuo. The residue was poured onto ice (ca. 100 g) and extracted with EtOAc ($\times 2$). The combined organic phase was washed with 1 N HCl several times, until *N,N*-dimethylaniline was completely removed, and then washed with water and brine. The organic phase was dried over anhydrous Na_2SO_4 , concentrated in vacuo, and purified by silica gel column chromatography to give compound 4.

5,7-Dichloropyrazolo[1,5-*a*]pyrimidine (13). 3-Aminopyrazole (4.2 g, 50 mmol) was reacted with diethyl malonate (8.1 g, 50 mmol) according to the general procedures A and B. The crude product was purified by silica gel column chromatography (hexane/EtOAc = 10:1) to give the title compound (3.0 g, 16 mmol, yield: 32% for two steps). ^1H NMR (CDCl_3) δ : 8.23 (1H, d, $J = 2.4$ Hz), 7.00 (1H, s), 6.75 (1H, d, $J = 2.4$ Hz). HRMS calcd for $\text{C}_6\text{H}_4\text{Cl}_2\text{N}_3$ ($\text{M} + \text{H}$) $^+$, 187.9777; found, 187.9768.

5,7-Dichloro-6-methylpyrazolo[1,5-*a*]pyrimidine (4e). 3-Aminopyrazole (2.2 g, 26 mmol) was reacted with diethyl methylmalonate (4.6 g, 26 mmol) according to the general procedure A and B. The crude product was purified by silica gel column chromatography (hexane/EtOAc = 10:1) to give the title compound (2.2 g, 11 mmol, yield: 42% for two steps). ^1H NMR (CDCl_3) δ : 8.16 (1H, d, $J = 2.4$ Hz), 6.71 (1H, d, $J = 2.4$ Hz), 2.56 (3H, s). HRMS calcd for $\text{C}_7\text{H}_6\text{Cl}_2\text{N}_3$ ($\text{M} + \text{H}$) $^+$, 201.9933; found, 201.9935.

General Procedure C for the Synthesis of Compound 5. To a stirred solution of a compound 4 (5.0 mmol) in 2-propanol (50 mL)

containing triethylamine (10 mmol) was added the appropriate amine (6.0 mmol). The reaction was heated for 15 h at 80 °C and cooled to room temperature. In the case that a precipitate was formed, this was collected by filtration and washed with MeOH. The solid was dried under vacuum to give compound 5. This product was used in the next reaction without further purification. In the case that a precipitate did not form, the reaction mixture was cooled to room temperature, the residue was partitioned between water and EtOAc, and the organic phase was separated. The aqueous phase was extracted with EtOAc (×2). The combined organic phase was washed with water and brine, dried over anhydrous Na₂SO₄, concentrated in vacuo, and purified by silica gel column chromatography to give compound 5.

General Procedure D for the Synthesis of Compound 5. To a stirred suspension of sodium hydride (3.0 mmol) in DMF (10 mL) were added the appropriate amine (2.4 mmol) and then a compound 4 (2.0 mmol) in THF (10 mL). The resulting mixture was stirred at room temperature to 50 °C for 2 h. The reaction was quenched with a saturated aqueous solution of NH₄Cl. After extraction with EtOAc, the combined organic phase was washed with water and brine, dried over anhydrous Na₂SO₄, and concentrated in vacuo. The crude product was purified by washing with MeOH or by silica gel column chromatography to give a compound 5.

5-Chloro-*N*-(3-chloro-4-fluorophenyl)pyrazolo[1,5-*a*]pyrimidin-7-amine (5a). 5,7-Dichloropyrazolo[1,5-*a*]pyrimidine (13) (0.51 g, 2.7 mmol) was reacted with 3-chloro-4-fluoroaniline (0.47 g, 3.3 mmol) according to the general procedure C to give the title compound (0.69 g, 2.3 mmol, yield: 85%). ¹H NMR (CDCl₃) δ: 8.07–8.04 (2H, m), 7.48–7.45 (1H, m), 7.32–7.28 (2H, m), 6.54–6.53 (1H, m), 6.18 (1H, s). HRMS calcd for C₁₂H₈Cl₂FN₄ (M + H)⁺, 297.0105; found, 297.0107.

***N*-(4-(Benzyloxy)phenyl)-5-chloro-6-methylpyrazolo[1,5-*a*]pyrimidin-7-amine (5p).** 5,7-Dichloro-6-methylpyrazolo[1,5-*a*]pyrimidine (4e) (0.25 g, 1.2 mmol) was reacted with 4-benzyloxyaniline (0.30 g, 1.5 mmol) according to the general procedure C to give the title compound (0.36 g, 0.98 mmol, yield: 82%). ¹H NMR (CDCl₃) δ: 8.07 (1H, s), 8.00 (1H, d, *J* = 2.4 Hz), 7.46–7.35 (5H, m), 7.13–7.09 (2H, m), 7.02–6.98 (2H, m), 6.49 (1H, d, *J* = 2.4 Hz), 5.09 (2H, s), 1.90 (3H, s). HRMS calcd for C₂₀H₁₈ClN₄O (M + H)⁺, 365.1164; found, 365.1153.

Ethyl 3-({5-Chloro-6-methylpyrazolo[1,5-*a*]pyrimidin-7-yl}amino)benzoate (5r). 5,7-Dichloro-6-methylpyrazolo[1,5-*a*]pyrimidine (4e) (0.25 g, 1.2 mmol) was reacted with ethyl 3-amino-benzoate (0.25 g, 1.5 mmol) according to the general procedure C to give the title compound (0.32 g, 0.98 mmol, yield: 82%). ¹H NMR (CDCl₃) δ: 8.10 (1H, s), 8.02 (1H, d, *J* = 2.2 Hz), 7.92–7.90 (1H, m), 7.77–7.75 (1H, m), 7.48 (1H, t, *J* = 7.9 Hz), 7.28 (1H, dd, *J* = 7.9, 2.2 Hz), 6.55 (1H, d, *J* = 2.2 Hz), 4.40 (2H, q, *J* = 7.2 Hz), 1.95 (3H, s), 1.41 (3H, t, *J* = 7.2 Hz). HRMS calcd for C₁₆H₁₆ClN₄O₂ (M + H)⁺, 331.0956; found, 331.0949.

5-Chloro-*N*-(2-chlorophenyl)-6-methylpyrazolo[1,5-*a*]pyrimidin-7-amine (5x). 5,7-Dichloro-6-methylpyrazolo[1,5-*a*]pyrimidine (4e) (0.25 g, 1.2 mmol) was reacted with 2-chloroaniline (0.19 g, 1.5 mmol) according to the general procedure D to give the title compound (0.22 g, 0.77 mmol, yield: 64%). ¹H NMR (CDCl₃) δ: 8.04 (1H, d, *J* = 2.4 Hz), 7.95 (1H, s), 7.51 (1H, dd, *J* = 7.9, 1.5 Hz), 7.30 (1H, td, *J* = 7.9, 1.5 Hz), 7.18 (1H, td, *J* = 7.9, 1.5 Hz), 7.03 (1H, dd, *J* = 7.9, 1.5 Hz), 6.56 (1H, d, *J* = 2.4 Hz), 1.95 (3H, s). HRMS calcd for C₁₃H₁₁Cl₂N₄ (M + H)⁺, 293.0355; found, 293.0342.

General Procedure E for the Synthesis of Compound 6. To a stirred solution of compound 5 (1.0 mmol) in 1,4-dioxane (5.0 mL) was added di-*tert*-butyl dicarbonate (2.0 mmol) followed by a catalytic amount of 4-dimethylaminopyridine. The reaction mixture was stirred at room temperature for 3 h. If starting material was detected by TLC, the reaction mixture was warmed to 60 °C and stirred for further 3 h. The reaction mixture was concentrated in vacuo. The residue was purified by silica gel column chromatography to give compound 6.

***tert*-Butyl *N*-(3-Chloro-4-fluorophenyl)-*N*-(5-chloropyrazolo[1,5-*a*]pyrimidin-7-yl) carbamate (6a).** 5-Chloro-*N*-(3-chloro-4-fluorophenyl)pyrazolo[1,5-*a*]pyrimidin-7-amine (5a) (0.30 g, 1.0 mmol)

was reacted with di-*tert*-butyl dicarbonate (0.44 g, 2.0 mmol) according to the general procedure E. The crude product was purified by silica gel column chromatography (hexane/EtOAc = 8/1) to give the title compound (0.33 g, 0.83 mmol, yield: 83%). ¹H NMR (CDCl₃) δ: 8.16 (1H, d, *J* = 2.4 Hz), 7.45 (1H, dd, *J* = 6.3, 2.4 Hz), 7.26–7.22 (1H, m), 7.13 (1H, t, *J* = 8.5 Hz), 6.72–6.69 (2H, m), 1.37 (9H, s).

***tert*-Butyl *N*-(5-Chloro-6-methylpyrazolo[1,5-*a*]pyrimidin-7-yl)-*N*-(4-ethoxyphenyl)carbamate (6m).** 5-Chloro-*N*-(4-ethoxyphenyl)-6-methylpyrazolo[1,5-*a*]pyrimidin-7-amine (5n) (1.0 g, 3.3 mmol) was reacted with di-*tert*-butyl dicarbonate (1.4 g, 6.6 mmol) according to the general procedure E. The crude product was purified by silica gel column chromatography (hexane/EtOAc = 8/1) to give the title compound (1.1 g, 2.8 mmol, yield: 85%). ¹H NMR (CDCl₃) δ: 8.10 (1H, s), 7.25–7.20 (2H, m), 6.82 (2H, d, *J* = 8.8 Hz), 6.65 (1H, d, *J* = 2.0 Hz), 3.99 (2H, q, *J* = 6.9 Hz), 2.31 (3H, s), 1.39–1.32 (12H, m).

***tert*-Butyl *N*-(4-(Benzyloxy)phenyl)-*N*-(5-chloro-6-methylpyrazolo[1,5-*a*]pyrimidin-7-yl)carbamate (6o).** *N*-(4-(Benzyloxy)phenyl)-5-chloro-6-methylpyrazolo[1,5-*a*]pyrimidin-7-amine (5p) (0.36 g, 0.98 mmol) was reacted with di-*tert*-butyl dicarbonate (0.43 g, 2.0 mmol) according to the general procedure E. The crude product was purified by silica gel column chromatography (hexane/EtOAc = 8/1) to give the title compound (0.37 g, 0.80 mmol, yield: 82%). ¹H NMR (CDCl₃) δ: 8.10 (1H, d, *J* = 2.2 Hz), 7.41–7.31 (5H, m), 7.25–7.21 (2H, m), 6.90 (2H, d, *J* = 8.8 Hz), 6.65 (1H, d, *J* = 2.2 Hz), 5.02 (2H, s), 2.31 (3H, s), 1.30 (9H, s).

***tert*-Butyl *N*-(5-Chloro-6-methylpyrazolo[1,5-*a*]pyrimidin-7-yl)-*N*-(2-methyl-1,3-benzothiazol-6-yl)carbamate (6u).** *N*-(5-Chloro-6-methylpyrazolo[1,5-*a*]pyrimidin-7-yl)-2-methyl-1,3-benzothiazol-6-amine (5v) (0.32 g, 0.98 mmol) was reacted with di-*tert*-butyl dicarbonate (0.43 g, 2.0 mmol) according to the general procedure E. The crude product was purified by silica gel column chromatography (hexane/EtOAc = 8/1) to give the title compound (0.29 g, 0.67 mmol, yield: 68%). ¹H NMR (CDCl₃) δ: 8.12 (1H, d, *J* = 2.2 Hz), 7.88 (1H, d, *J* = 8.8 Hz), 7.78 (1H, s), 7.35 (1H, d, *J* = 8.8 Hz), 6.69 (1H, d, *J* = 2.2 Hz), 2.82 (3H, s), 2.32 (3H, s), 1.35 (9H, s).

General Procedure F for the Synthesis of Compound 9. A mixture of the compound 6 (1.0 mmol) and appropriate amine (1.0 g) was heated at 80–85 °C for 18 h. If the amine was not liquid at this reaction temperature, MeCN was added as a solvent. The crude material was then partitioned between EtOAc and water. The organic phase was then separated and washed with water and brine, dried over anhydrous Na₂SO₄, and concentrated in vacuo. The residue was dissolved in CH₂Cl₂ (5.0 mL) and TFA (3.0 mL). The reaction mixture was stirred for 1 h at room temperature and then evaporated in vacuo. The residue was partitioned between EtOAc and a saturated aqueous solution of NaHCO₃. The organic phase was separated, washed with water and brine, dried over anhydrous Na₂SO₄, and concentrated in vacuo. The residue was purified by preparative HPLC. To get a salt-free product, the purified product was dissolved in EtOAc and washed with saturated aqueous solution of NaHCO₃ and brine, dried over anhydrous Na₂SO₄, and concentrated in vacuo to give the title compound.

5-*N*-(trans-4-Aminocyclohexyl)-7-*N*-(3-chloro-4-fluorophenyl)pyrazolo[1,5-*a*]pyrimidine-5,7-diamine (1). *tert*-Butyl *N*-(3-chloro-4-fluorophenyl)-*N*-(5-chloropyrazolo[1,5-*a*]pyrimidin-7-yl)carbamate (6a) (0.40 g, 1.0 mmol) was reacted with *trans*-1,4-cyclohexanediamine (1.0 g, 8.8 mmol) according to the general procedure F to get the title compound (0.20 g, 0.53 mmol, yield: 53%). ¹H NMR (DMSO-*d*₆) δ: 7.80 (1H, d, *J* = 2.0 Hz), 7.60 (1H, dd, *J* = 6.8, 2.4 Hz), 7.48 (1H, t, *J* = 9.0 Hz), 7.42–7.38 (1H, m), 6.77 (1H, d, *J* = 7.8 Hz), 5.94 (1H, d, *J* = 2.0 Hz), 5.57 (1H, s), 3.68 (1H, s), 2.85–2.80 (1H, m), 1.96–1.85 (4H, m), 1.34–1.11 (4H, m). HRMS calcd for C₁₈H₂₁ClFN₆ (M + H)⁺, 375.1495; found, 375.1497.

7-*N*-(4-Ethoxyphenyl)-6-methyl-5-*N*-(*S*-piperidin-3-yl)pyrazolo[1,5-*a*]pyrimidine-5,7-diamine (44). *tert*-Butyl *N*-(5-chloro-6-methylpyrazolo[1,5-*a*]pyrimidin-7-yl)-*N*-(4-ethoxyphenyl)carbamate (6m) (0.50 g, 1.2 mmol) was reacted with 3-amino-1-Boc-piperidine (1.0 g, 5.0 mmol) according to the general procedure

F to get the title compound. For the syntheses of (*rac*)-**44**, (*S*)-**44**, and (*R*)-**44**, (\pm)-3-amino-1-Boc-piperidine, (*S*)-3-amino-1-Boc-piperidine, [pyrimidin-7-yl] and (*R*)-3-amino-1-Boc-piperidine were used respectively (0.25 g, 0.68 mmol, yield: 57% for (*S*)-**44**, (*rac*)-**44** and (*R*)-**44** gave similar yields). $^1\text{H NMR}$ (DMSO- d_6) δ : 8.54 (1H, s), 7.75 (1H, d, $J = 2.0$ Hz), 6.90–6.83 (4H, m), 6.05 (1H, d, $J = 7.8$ Hz), 5.98 (1H, d, $J = 2.0$ Hz), 4.17 (1H, s), 3.96 (2H, q, $J = 6.8$ Hz), 3.17 (1H, d, $J = 7.8$ Hz), 2.96–2.93 (1H, m), 2.58–2.52 (2H, m), 1.91–1.86 (1H, m), 1.74–1.70 (1H, m), 1.65 (3H, s), 1.57–1.52 (2H, m), 1.30 (3H, t, $J = 6.8$ Hz). HRMS calcd for $\text{C}_{20}\text{H}_{27}\text{N}_6\text{O}$ ($\text{M} + \text{H}$) $^+$, 367.2241; found, 367.2243.

6-Methyl-7-N-(2-methyl-1,3-benzothiazol-6-yl)-5-N-(S-piperidin-3-yl)pyrazolo[1,5-a]pyrimidine-5,7-diamine (64). *tert*-Butyl *N*-{5-chloro-6-methylpyrazolo[1,5-*a*]pyrimidin-7-yl}-*N*-(2-methyl-1,3-benzothiazol-6-yl)carbamate (**6u**) (0.15 g, 0.35 mmol) was reacted with (*S*)-3-amino-1-Boc-piperidine (1.0 g, 5.0 mmol) according to the general procedure F to get the title compound (66 mg, 0.17 mmol, yield: 49%). $^1\text{H NMR}$ (DMSO- d_6) δ : 8.93 (1H, s), 7.76 (1H, d, $J = 8.8$ Hz), 7.74 (1H, d, $J = 2.2$ Hz), 7.37 (1H, d, $J = 2.2$ Hz), 7.10 (1H, dd, $J = 8.8, 2.2$ Hz), 6.10 (1H, d, $J = 7.8$ Hz), 6.02 (1H, d, $J = 2.2$ Hz), 4.15–4.07 (1H, m), 3.12 (1H, dd, $J = 12.0, 3.4$ Hz), 2.88–2.85 (1H, m), 2.72 (3H, s), 2.53–2.47 (2H, m), 1.88 (1H, s), 1.76 (3H, s), 1.72–1.65 (1H, m), 1.61–1.45 (2H, m). HRMS calcd for $\text{C}_{20}\text{H}_{24}\text{N}_7\text{S}$ ($\text{M} + \text{H}$) $^+$, 394.1808; found, 394.1807.

***tert*-Butyl (S)-3-[(7-[(*tert*-butoxy)carbonyl](4-ethoxyphenyl)amino)-6-methylpyrazolo[1,5-*a*]pyrimidin-5-yl]aminopiperidine-1-carboxylate (8a)**. A mixture of *tert*-butyl *N*-{5-chloro-6-methylpyrazolo[1,5-*a*]pyrimidin-7-yl}-*N*-(4-ethoxyphenyl)carbamate (**6m**) (0.40 g, 0.99 mmol) and (*S*)-3-amino-1-Boc-piperidine (2.0 g, 10 mmol) was heated together at 80–85 °C for 18 h. The reaction mixture was cooled to room temperature and was directly purified by silica gel column chromatography (hexane/EtOAc = 8/1) to give the title compound (0.43 g, 0.76 mmol, yield: 77%). $^1\text{H NMR}$ (CDCl_3) δ : 7.84 (1H, d, $J = 2.0$ Hz), 7.29–7.26 (2H, m), 6.81–6.79 (2H, m), 6.16 (1H, d, $J = 2.0$ Hz), 4.22 (1H, s), 3.98 (2H, q, $J = 7.0$ Hz), 3.78–3.22 (4H, m), 2.02 (3H, s), 1.91–1.83 (2H, m), 1.73–1.61 (2H, m), 1.50–1.30 (21H, m).

***tert*-Butyl (S)-3-[(7-[(4-(benzyloxy)phenyl)](*tert*-butoxy)carbonyl]amino)-6-methylpyrazolo[1,5-*a*]pyrimidin-5-yl]aminopiperidine-1-carboxylate (15)**. *tert*-Butyl *N*-[4-(benzyloxy)phenyl]-*N*-{5-chloro-6-methylpyrazolo[1,5-*a*]pyrimidin-7-yl}-carbamate (**6o**) (0.47 g, 1.0 mmol) was reacted with (*S*)-3-amino-1-Boc-piperidine (2.0 g, 10 mmol) according to an analogous fashion to **8a**. The reaction mixture was purified by silica gel column chromatography (hexane/EtOAc = 8/1) to give the title compound (0.43 g, 0.68 mmol, yield: 68%). $^1\text{H NMR}$ (CDCl_3) δ : 7.84 (1H, d, $J = 2.0$ Hz), 7.40–7.29 (7H, m), 6.88 (2H, dd, $J = 8.8, 2.0$ Hz), 6.16 (1H, d, $J = 2.0$ Hz), 5.01 (2H, s), 4.22 (1H, s), 3.82–3.16 (4H, m), 2.02 (3H, s), 1.88 (1H, s), 1.77–1.56 (3H, m), 1.48–1.29 (18H, m).

7-N-[4-(2-Methoxyethoxy)phenyl]-6-methyl-5-N-(S)-piperidin-3-yl]pyrazolo[1,5-*a*]pyrimidine-5,7-diamine (59). To a stirred solution of *tert*-butyl (S)-3-[(7-[(4-(benzyloxy)phenyl)](*tert*-butoxy)carbonyl]amino)-6-methylpyrazolo[1,5-*a*]pyrimidin-5-yl]aminopiperidine-1-carboxylate (**15**) (1.0 g, 1.6 mmol) in MeOH (50 mL) was added Pd(OH) $_2$ /C (50 mg, 10% on carbon) under nitrogen atmosphere. The reaction mixture was stirred at room temperature for 16 h under hydrogen atmosphere, and Pd(OH) $_2$ /C was filtered off. The solvent was removed in vacuo to give the crude alcohol product **16** (0.81 g, 1.5 mmol, yield: 94%). This crude product was used in the next reaction without further purification.

To a stirred solution of crude product **16** (81 mg, 0.15 mmol), 2-methoxyethanol (23 mg, 0.30 mmol), and triphenylphosphine (52 mg, 0.20 mmol) in THF (5.0 mL) was added a solution of diisopropyl azodicarboxylate (43 mg, 0.21 mmol) in toluene (0.11 mL) at 0 °C. The reaction mixture was stirred at room temperature for 10 h. The reaction was quenched by addition of water. EtOAc was added, and the organic phase was separated. The aqueous phase was extracted with EtOAc ($\times 2$), and the combined organic phase was washed with water and brine, dried over anhydrous Na_2SO_4 , and concentrated in

vacuo. The residue was dissolved in CH_2Cl_2 (2.0 mL). To this solution was added TFA (1.0 mL), and the reaction mixture was stirred for 3 h. The solvent was removed in vacuo. The residue was purified by preparative HPLC. To get a salt-free product, the purified product was dissolved in EtOAc, washed with a saturated aqueous solution of NaHCO_3 and brine, dried over anhydrous Na_2SO_4 , and concentrated in vacuo to give the title compound (13 mg, 0.032 mmol, yield: 20% for two steps from **16**). $^1\text{H NMR}$ (DMSO- d_6) δ : 8.50 (1H, s), 7.73 (1H, d, $J = 2.0$ Hz), 6.91–6.84 (4H, m), 5.97 (1H, d, $J = 2.0$ Hz), 5.95 (1H, d, $J = 7.8$ Hz), 4.10–4.01 (3H, m), 3.64–3.62 (2H, m), 3.29 (3H, s), 3.07 (1H, dd, $J = 11.7, 3.2$ Hz), 2.85–2.80 (1H, m), 2.49–2.42 (2H, m), 1.89–1.82 (1H, m), 1.67–1.64 (1H, m), 1.66 (3H, s), 1.59–1.41 (2H, m). HRMS calcd for $\text{C}_{21}\text{H}_{29}\text{N}_6\text{O}_2$ ($\text{M} + \text{H}$) $^+$, 397.2347; found, 397.2338.

General Procedure G for Measurement of Enzyme Activity Inhibition. Compound Preparation. Compounds were dissolved in DMSO at a concentration of 10 mM and stored in aliquots at –20 °C. Compounds in DMSO from these stock aliquots were diluted in DMSO to produce the required range of 30 \times stock solutions. These stock solutions were then subjected to 1:3 dilutions to prepare the required range of 10 \times stock solutions, and 5 μL of each solution was used in each 50 μL reaction. A final DMSO concentration of 3% was maintained throughout all compound dilution series to maximize compound solubility. Compounds were routinely tested at final concentrations ranging from 300 μM to 0.001 μM but may have been tested at lower concentrations depending upon their activity.

MAPKAP-K2 Assay. The kinase reaction was conducted in a round-bottomed polypropylene 96-well plate. MAPKAP-kinase 2 was diluted to 0.5 mU/ μL in diluent buffer (50 mM Tris/HCl, pH 7.5, 0.1 mM EGTA, 0.1% (v/v) β -mercaptoethanol, 1 mg/mL BSA). Five microliters of compound or 30% DMSO was added to each well followed by 25 μL of substrate cocktail (final concentration: 10 μM ATP, 30 μM peptide (KKLNRTLSSVA), 0.5 μCi of ^{33}P - γ -ATP (or 1 μCi for kinetic determinations) in 50 mM Tris pH 7.5, 0.1 mM EGTA, 10 mM Mg-acetate, and 0.1% β -mercaptoethanol). The reaction was initiated with the addition of 20 μL of enzyme solution per well or 20 μL of diluent buffer without enzyme. The plate was shaken for 10 s and then left at room temperature for 30 min. The reaction was terminated with 50 μL of 150 mM phosphoric acid. An amount of 90 μL of the reaction mixture was then transferred into a 96-well P81 filter plate (Whatmann) and incubated at room temperature for 5 min. The filter plate was then washed four times with 200 μL of 75 mM phosphoric acid per well on a plate vacuum manifold (Millipore) and dried in an oven for 2–3 h. Packard MicroScint 'O' (30 μL) was then added to each well, and the plate was mixed for 30 min and subjected to liquid scintillation counting on a Packard TopCount.

CDK2 Assay. The kinase reaction was conducted in a round-bottomed polypropylene 96-well plate. CDK2 was diluted to 0.5 ng/ μL in diluent buffer (50 mM Tris/HCl, pH 7.5, 0.1 mM EGTA, 0.1% (v/v) β -mercaptoethanol, 1 mg/mL BSA). Five microliters of compound or 30% DMSO was added to each well followed by 25 μL of substrate cocktail (final 10 μM ATP, 0.1 mg/mL histone type III-S, 0.2 μCi ^{33}P - γ -ATP in 50 mM Tris-HCl (pH 7.5), 1 mM EGTA, 2 mM DTT, 10 mM MgCl_2 , 0.01% Brij-35). The reaction was initiated with the addition of 20 μL of enzyme solution per well or 20 μL of diluent buffer without enzyme. The plate was shaken for 10 s and then left at room temperature for 60 min. The reaction was terminated with 50 μL of 150 mM phosphoric acid. An amount of 90 μL of the reaction mixture was then transferred into a 96-well P81 filter plate (Whatman) and incubated at room temperature for 5 min. The filter plate was then washed four times with 200 μL of 75 mM phosphoric acid per well on a plate vacuum manifold (Millipore) and dried in an oven for 2–3 h. Packard MicroScint 'O' (30 μL) was then added to each well, the plate was mixed for 30 min and subjected to liquid scintillation counting on a Packard TopCount.

LPS-Induced TNF- α Production in THP-1 Cells. THP-1 cells (ATCC: TIB-202) were suspended in THP-1 media (90% RPMI 1640 containing 2 mM L-glutamine, 1.5 g/L sodium bicarbonate, 4.5 g/L

D-glucose, 10 mM HEPES, 1 mM sodium pyruvate, 0.05 mM 2-ME, 10% heat-inactivated FBS) at a density of 1×10^5 cells/mL. An amount of 100 μ L of THP-1 cell suspension was then plated in a 96-well tissue culture plate and incubated in a CO₂ incubator for 2 h. Cells were pretreated for 1 h in a CO₂ incubator in the presence of a further 40 μ L of THP-1 media and 50 μ L of test compound (serial dilutions in DMSO). LPS was then added (10 μ g/mL final), and the cells were further incubated for 18 h. The cell supernatants were harvested and measured for TNF- α concentration using a HTRF Human TNF- α kit (CisBio). Compound effects on cell growth during the assay period were assessed by assaying residual cells with the CellTiter 96 Aqueous One Solution Reagent (Promega).

Whole Blood Assays. Mouse whole blood or human whole blood (from two healthy and nonmedicated volunteers in the latter case) was drawn and diluted four times in RPMI-1640. Diluted blood (360 μ L per well) was dispensed into 48-well plates and test compound (0.4–100 μ M) added in DMSO (20 μ L). LPS (10 μ g/mL) was added prior to an overnight incubation. The concentrations of TNF- α in the cell supernatants were measured by using an ELISA (R&D Systems, Inc.).

LPS-Induced HSP27 Phosphorylation in THP-1 Cells. THP-1 cells (5×10^5 cells/dish) were incubated in a CO₂ incubator for 1 h. The cells were then preincubated in the presence of test compound ((S)-44: 3 μ M and 30 μ M; BIRB796: 0.1 μ M) for 1 h. After addition of LPS (10 μ g/mL), the cells were further incubated for 1 h and then washed with PBS. Following lysis at 4 °C for 15 min, lysates were centrifuged and then subjected to SDS-PAGE analysis (20 μ g protein/lane) followed by protein transfer and immunoblotting with an antiphospho-specific antibody (Cell Signaling Technology).

Pharmacokinetics. The iv and po pharmacokinetic profile were investigated at a dose of 1 mg/kg in male mice. Formulations were 0.5% Tween 80 in saline for iv dosing and 0.5% methyl cellulose aqueous solution for po dosing. The plasma concentration was measured by LC/MS/MS after serial blood sampling. The individual pharmacokinetic parameters were calculated by noncompartmental analysis and the mean parameters calculated. AUC_{0–24} is the area under plasma concentration–time curve from time 0 to 24 h after oral administration. CL_{tot} is the plasma total clearance obtained from iv administration.

Effect of (S)-44 on TNF- α Production in Murine Endotoxin Shock Model. Vehicle (5 mM HCl/saline) or 10, 30, 60, or 100 mg/kg body weight of (S)-44 (5 mM HCl/saline) (n = 6) was administered orally to C57BL/6 mice (male, 8 week old; Charles River Japan). Thirty minutes later, 0.5 mg/kg body weight of lipopolysaccharide (LPS; E. coli 055:B5, Sigma-Aldrich Co.) was administered intraperitoneally. Sixty minutes after the LPS administration, blood was collected through the abdominal vein under barbiturate anesthesia. Serum was prepared for measurement of TNF- α concentration by the ELISA method (R&D Systems, Inc.). Statistical analysis was carried out with the Dunnett's multiple comparison test, with $P < 0.05$ being considered as significant.

■ ASSOCIATED CONTENT

📄 Supporting Information

Experimental details for the synthesis of all compounds and spectral data of all intermediates and final compounds. Kinase selectivity panel for (S)-44. THP-1 cell based assay concentration effect curves for (S)-44, 59, and 64. This material is available free of charge via the Internet at <http://pubs.acs.org>.

Accession Codes

†PDB ID 3A2C.

■ AUTHOR INFORMATION

Corresponding Author

*(G.U.) Phone +81-42-586-8267; e-mail: g.unoki@teijin.co.jp. (D.R.M.) Phone: +44-1799-533500; e-mail: dale.mitchell@glp.com.

Present Addresses

[†]GlaxoSmithKline Medicines Research Centre, Gunnels Wood Road, Stevenage, Hertfordshire, SG1 2NY, U.K.

[#]Computational and Structural Chemistry, GlaxoSmithKline Medicines Research Centre, Gunnels Wood Rd., Stevenage, Hertfordshire, SG1 2NY, U.K.

[▽]Merck Research Laboratories, 2000 Galloping Hill Rd., Kenilworth, NJ 07033.

Notes

The authors declare no competing financial interest.

■ ABBREVIATIONS USED

MAPKAP-K2, mitogen-activated protein kinase-activated protein kinase 2; CDK2, cyclin dependent kinase 2; TNF- α , tumor necrosis factor- α ; MAP, mitogen-activated protein; SAR, structure–activity relationship; Ser, serine; Thr, threonine; mRNA, messenger ribonucleic acid; SFK, SoftFocus kinase; Boc, butyloxycarbonyl; ATP, adenosine triphosphate; cAMP, cyclic adenosine monophosphate; Leu, leucine; Asn, asparagine; Asp, aspartic acid; Phe, phenylalanine; ADP, adenosine diphosphate; Glu, glutamic acid; Cys, cysteine; CDK1, cyclin dependent kinase 1; ERK2, extracellular signal-regulated kinase 2; IKK β , inhibitor of nuclear factor kappa-B kinase subunit beta; JNK1 α 1, c-Jun N-terminal kinase 1 alpha 1; JNK2 α 2, c-Jun N-terminal kinase 2 alpha 2; p38 α , mitogen-activated protein kinase p38 alpha; p38 β , mitogen-activated protein kinase p38 beta; p38 γ , mitogen-activated protein kinase p38 gamma; p38 δ , mitogen-activated protein kinase p38 delta; MKK4, mitogen-activated protein kinase kinase 4; MKK6, mitogen-activated protein kinase kinase 6; MKK7 β , mitogen-activated protein kinase kinase 7 beta; MEK1, dual specificity mitogen-activated protein kinase kinase 1; AMPK, 5' adenosine monophosphate-activated protein kinase; CaMK2, calmodulin-dependent protein kinase 2; CaMK4, calmodulin-dependent protein kinase 4; CHK1, checkpoint kinase 1; CHK2, checkpoint kinase 2; PKB α , protein kinase B alpha; p70S6K, 70 kDa ribosomal protein S6 kinase 1; PDK1, 3-phosphoinositide-dependent protein kinase 1; PKA, protein kinase A; PKC α , protein kinase C alpha; PKC γ , protein kinase C gamma; ROCK-II, Rho-associated kinase 2; Rsk2, ribosomal protein S6 kinase 2; PRAK, p38-regulated and activated kinase; LPS, lipopolysaccharide

■ REFERENCES

- (1) Camussi, G.; Lupia, E. The future role of anti-tumor necrosis factor (TNF) products in the treatment of rheumatoid arthritis. *Drugs* **1998**, *55* (5), 613–620.
- (2) Braun, J.; Sieper, J. Role of novel biological therapies in psoriatic arthritis: Effects on joints and skin. *BioDrugs* **2003**, *17* (3), 187–199.
- (3) Jarvis, B.; Faulds, D. Etanercept: A review of its use in rheumatoid arthritis. *Drugs* **1999**, *57* (6), 945–966.
- (4) Richard-Miceli, C.; Dougados, M. Tumour necrosis factor- α blockers in rheumatoid arthritis: Review of the clinical experience. *BioDrugs* **2001**, *15* (4), 251–259.
- (5) Seymour, H. E.; Worsley, A.; Smith, J. M.; Thomas, S. H. L. Anti-TNF agents for rheumatoid arthritis. *Br. J. Clin. Pharmacol.* **2001**, *51* (3), 201–208.
- (6) Adams, J. L.; Badger, A. M.; Kumar, S.; Lee, J. C. p38 MAP kinase: Molecular target for the inhibition of pro-inflammatory cytokines. *Prog. Med. Chem.* **2001**, *38*, 1–60.
- (7) Lee, J. C.; Laydon, J. T.; McDonnell, P. C.; Gallagher, T. F.; Kumar, S.; Green, D.; McNulty, D.; Blumenthal, M. J.; Heyes, J. R.; Landvatter, S. W.; Strickler, J. E.; McLaughlin, M. M.; Siemens, I. R.; Fisher, S. M.; Livi, G. P.; White, J. R.; Adams, J. L.; Young, P. R. A

protein kinase involved in the regulation of inflammatory cytokine biosynthesis. *Nature (London)* **1994**, 372 (6508), 739–746.

(8) Regan, J.; Breitfelder, S.; Cirillo, P.; Gilmore, T.; Graham, A. G.; Hickey, E.; Klaus, B.; Madwed, J.; Moriak, M.; Moss, N.; Pargellis, C.; Pav, S.; Proto, A.; Swinamer, A.; Tong, L.; Torcellini, C. Pyrazole urea-based inhibitors of p38 MAP kinase: from lead compound to clinical candidate. *J. Med. Chem.* **2002**, 45, 2994–3008.

(9) Tamura, K.; Sudo, T.; Senthleben, U.; Dadak, A. M.; Johnson, R.; Karin, M. Requirement for p38alpha in erythropoietin expression: a role for stress kinases in erythropoiesis. *Cell* **2000**, 102, 221.

(10) Adams, R. H.; Porras, A.; Alonso, G.; Jones, M.; Vintersten, K.; Panelli, S.; Valladares, A.; Perez, L.; Klein, R.; Nebreda, A. R. Essential role of p38alpha MAP kinase in placental but not embryonic cardiovascular development. *Mol. Cell* **2000**, 6, 109–116.

(11) Cohen, P. Targeting protein kinases for the development of antiinflammatory drugs. *Curr. Opin. Cell Biol.* **2009**, 317–324.

(12) Kotlyarov, A.; Neining, A.; Schubert, C.; Eckert, R.; Birmeyer, C.; Volk, H.-D.; Gaestel, M. MAPKAP kinase 2 is essential for LPS induced TNF- α biosynthesis. *Nat. Cell Biol.* **1999**, 1 (2), 94–97.

(13) Winzen, R.; Kracht, M.; Ritter, B.; Wilhelm, A.; Chen, C.-Y. A.; Shyu, A.-B.; Muller, M.; Gaestel, M.; Resch, K.; Holtmann, H. The p38 MAP kinase pathway signals for cytokine-induced mRNA stabilization via MAP kinase-activated protein kinase 2 and an AU-rich region-targeted mechanism. *EMBO J.* **1999**, 18 (18), 4969–4980.

(14) Gaestel, M. MAPKAP kinases - MKs - two's company, three's a crowd. *Nat. Rev. Mol. Cell Biol.* **2006**, 7 (2), 120–130.

(15) Ronkina, N.; Kotlyarov, A.; Dittrich-Breiholz, O.; Kracht, M.; Hitti, E.; Milarski, K.; Askew, R.; Marusic, S.; Lin, L.-L.; Gaestel, M.; Telliez, J.-B. The Mitogen-activated Protein Kinase (MAPK)-Activated Protein Kinases MK2 and MK3 Cooperate in Stimulation of Tumor Necrosis Factor Biosynthesis and Stabilization of p38 MAPK. *Mol. Cell Biol.* **2007**, 27, 170.

(16) Hegen, M.; Gaestel, M.; Nickerson-Nutter, C. L.; Lin, L. L.; Telliez, J. B. MAPKAP kinase 2-deficient mice are resistant to collagen-induced arthritis. *J. Immunol.* **2006**, 177, 1913–1917.

(17) Saklatvala, J. The p38 MAP kinase pathway as a therapeutic target in inflammatory disease. *Curr. Opin. Pharmacol.* **2004**, 4, 372–377.

(18) Neining, A.; Kontoyiannis, D.; Kotlyarov, A.; Winzen, R.; Eckert, R.; Volk, H.-D.; Holtmann, H.; Kollias, G.; Gaestel, M. MK2 Targets AU-rich Elements and Regulates Biosynthesis of Tumor Necrosis Factor and Interleukin-6 Independently at Different Post-translational Levels. *J. Biol. Chem.* **2002**, 277, 3065–3068.

(19) Damjanov, N.; Kauffman, R. S.; Spencer-Green, G. T. Efficacy, Pharmacodynamics and Safety of VX-702, a Novel p38 MAPK Inhibitor, in Rheumatoid Arthritis. *Arthritis Rheum.* **2009**, 5, 1232–1241.

(20) Clark, A. R.; Dean, J. L. E.; Saklatvala, J. The p38 MAPK pathway mediates both antiinflammatory and proinflammatory processes: comment on the article by Damjanov and the editorial by Genovese. *Arthritis Rheum.* **2009**, 5, 3513–3514.

(21) Anderson, D. R.; Hegde, S.; Reinhard, E.; Gomez, L.; Vernier, W. F.; Lee, L.; Liu, S.; Sambandam, A.; Snider, P. A.; Masih, L. Aminocyanopyridine inhibitors of mitogen activated protein kinase-activated protein kinase 2 (MK-2). *Bioorg. Med. Chem. Lett.* **2005**, 15, 1587–1590.

(22) Trujillo, J. I.; Meyers, M. J.; Anderson, D. R.; Hegde, S.; Mahoney, M. W.; Vernier, W. F.; Buchler, I. P.; Wu, K. K.; Yang, S.; Hartmann, S. J.; Reitz, D. B. Novel tetrahydro- β -carboline-1-carboxylic acids as inhibitors of mitogen activated protein kinase-activated protein kinase 2 (MK-2). *Bioorg. Med. Chem. Lett.* **2007**, 17, 4657–4663.

(23) Anderson, D. R.; Meyers, M. J.; Vernier, W. F.; Mahoney, M. W.; Kurumbail, R. G.; Caspers, N.; Poda, G. I.; Schindler, J. F.; Reitz, D. B.; Mourey, R. J. Pyrrolopyridine Inhibitors of Mitogen-Activated Protein Kinase-Activated Protein Kinase 2 (MK-2). *J. Med. Chem.* **2007**, 50, 2647–2654.

(24) Wu, J.-P.; Wang, J.; Abeywardane, A.; Andersen, D.; Emmanuel, M.; Gautschi, E.; Goldberg, D. R.; Kashem, M. A.; Lukas, S.; Mao, W.; Martin, L.; Morwick, T.; Moss, N.; Pargelis, C.; Patel, U. R.; Patnaude, L.; Peet, G. W.; Skow, D.; Snow, R. J.; Ward, Y.; Werneburg, B.; White, A. The discovery of carboline analogs as potent MAPKAP-K2 inhibitors. *Bioorg. Med. Chem. Lett.* **2007**, 17, 4664–4669.

(25) Goldberg, D. R.; Choi, Y.; Cogan, D.; Corson, M.; DeLeon, R.; Gao, A.; Gruenbaum, L.; Hao, M. H.; Joseph, D.; Kashem, M. A.; Miller, C.; Moss, N.; Netherton, M. R.; Pargellis, C. P.; Pelletier, J.; Sellati, R.; Skow, D.; Torcellini, C.; Tseng, Y.-C.; Wang, J.; Watsi, R.; Werneburg, B.; Wu, J. P.; Xiong, Z. Pyrazinoindolone inhibitors of MAPKAP-K2. *Bioorg. Med. Chem. Lett.* **2008**, 18, 938–941.

(26) Xiong, Z.; Gao, D. A.; Cogan, D. A.; Goldberg, M.-H. H.; Moss, N.; Pack, E.; Pargelis, C.; Skow, D.; Trieselmann, T.; Werneburg, B.; White, A. Synthesis and SAR studies of indole-based MK2 inhibitors. *Bioorg. Med. Chem. Lett.* **2008**, 18, 1994–1999.

(27) Schlapbach, A.; Feifel, R.; Hawtin, S.; Heng, R.; Koch, G.; Moebitz, H.; Revesz, L.; Scheufler, C.; Velcicky, J.; Waelchli, R.; Huppertz, C. Pyrrolo-pyrimidones: A novel class of MK2 inhibitors with potent cellular activity. *Bioorg. Med. Chem. Lett.* **2008**, 18, 6142–6146.

(28) Anderson, D. R.; Meyers, M. J.; Kurumbail, R. G.; Caspers, N.; Poda, G. I.; Long, S. A.; Pierce, B. S.; Mahoney, M. W.; Mourey, R. J. Benzothiophene inhibitors of MK2. Part 1: Structure–activity relationships, assessments of selectivity and cellular potency. *Bioorg. Med. Chem. Lett.* **2009**, 19, 4878–4881.

(29) Anderson, D. R.; Meyers, M. J.; Kurumbail, R. G.; Caspers, N.; Poda, G. I.; Long, S. A.; Pierce, B. S.; Mahoney, M. W.; Mourey, R. J.; Parikh, M. D. Benzothiophene inhibitors of MK2. Part 2: Improvements in kinase selectivity and cell potency. *Bioorg. Med. Chem. Lett.* **2009**, 19, 4882–4884.

(30) Schlapbach, A.; Huppertz, C. Low-molecular-weight MK2 inhibitors a tough nut to crack! *Future Med. Chem.* **2009**, 1 (7), 1243–1257.

(31) Revesz, L.; Schlapbach, A.; Aichholz, R.; Feifel, R.; Hawtin, S.; Heng, R.; Hiestand, P.; Jahnke, W.; Koch, G.; Kroemer, M.; Möbitz, H.; Scheufler, C.; Velcicky, J.; Huppertz, C. In vivo and in vitro SAR of tetracyclic MAPKAP-K2 (MK2) inhibitors. Part I. *Bioorg. Med. Chem. Lett.* **2010**, 20, 4715–4718.

(32) Revesz, L.; Schlapbach, A.; Aichholz, R.; Dawson, J.; Feifel, R.; Hawtin, S.; Littlewood-Evans, A.; Koch, G.; Kroemer, M.; Möbitz, H.; Scheufler, C.; Velcicky, J.; Huppertz, C. In vivo and in vitro SAR of tetracyclic MAPKAP-K2 (MK2) inhibitors. Part II. *Bioorg. Med. Chem. Lett.* **2010**, 20, 4719–4723.

(33) Mourey, R. J.; Burnette, B. L.; Brustkern, S. J.; Daniels, J. S.; Hirsch, J. L.; Hood, W. F.; Meyers, M. J.; Mnich, S. J.; Pierce, B. S.; Saabye, M. J.; Schindler, J. F.; South, S. A.; Webb, E. G.; Zhang, J.; Anderson, D. R. A Benzothiophene Inhibitor of Mitogen-Activated Protein Kinase-Activated Protein Kinase 2 Inhibits Tumor Necrosis Factor α Production and Has Oral Anti-Inflammatory Efficacy in Acute and Chronic Models of Inflammation. *J. Pharmacol. Exp. Ther.* **2010**, 333, 797–807.

(34) Kinase focused libraries from BioFocus were used. BioFocus URL: <http://www.biofocus.com/>

(35) The protein structure of Phosphorylase Kinase (PDB code: 1PHK) was used.

(36) The protein structure of cAMP-dependent protein kinase (PDB code: 1BX6, 1STC) was used.

(37) TRIPOS URL: <http://www.tripos.com/>

(38) The crystal structure of purvalnol B in CDK (PDB ID: 1CKP) was used.

(39) Williamson, D. S.; Parratt, M. J.; Bower, J. F.; Moore, J. D.; Richardson, C. M.; Dokurno, P.; Cansfield, A. D.; Francis, G. L.; Hebdon, R. J.; Howes, R.; Jackson, P. S.; Lockie, A. M.; Murray, J. B.; Nunns, C. L.; Powles, J.; Robertson, A.; Surgenor, A. E.; Torrance, C. J. Structure-guided design of pyrazolo[1,5-a]pyrimidines as inhibitors of human cyclin-dependent kinase 2. *Bioorg. Med. Chem. Lett.* **2005**, 15, 863–867.

(40) Fujino, A.; Fukushima, K.; Namiki, N.; Kosugi, T.; Takimoto-Kamimura, M. Structural analysis of an MK2-inhibitor complex: insight into the regulation of the secondary structure of the Gly-rich loop by TEI-I01800. *Acta Crystallogr.* **2010**, *66*, 80–87.

(41) Diskin, R.; Engelberg, D.; Livnah, O. A Novel Lipid-binding site formed by the MAP Kinase Insert in p38 α . *J. Mol. Biol.* **2008**, *375*, 70–79.

(42) Perry, J. J. P.; Harris, R. M.; Moiani, D.; Olson, A. J.; Tainer, J. A. p38 α . MAP Kinase C-Terminal Domain Binding Pocket Characterized by Crystallographic and Computational Analyses. *J. Mol. Biol.* **2009**, *391*, 1–11.

(43) Fujino, A. et al. Unpublished results.